Sperm fertility in mice with oligo-astheno-teratozoospermia restored by *in vivo* injection and electroporation of naked mRNA

Charline Vilpreux[1], Guillaume Martinez[1,4], Paul Fourquin[1], Magali Court[1], Florence Appaix[6], Jean-Luc Duteyrat[2], Maxime Henry[7], Julien Vollaire[7], Camille Ayad[3], Altan Yavuz[3], Lisa De Macedo[1], Geneviève Chevalier[1], Edgar Del Llano [1], Emeline Lambert[1], Sekou Ahmed Conte[1], Zeina Wehbe[1,4], Elsa Giordani[1], Véronique Josserand[7], Jacques Brocard[2], Coutton Charles[1,4], Bernard Verrier[3], Pierre F. Ray[1,5], Corinne Loeuillet[1], Christophe Arnoult[1] and Jessica Escoffier[1*].

[1] Université Grenoble Alpes, Inserm U1209, CNRS UMR 5309, Team Genetic, Epigenetic and Therapies of infertility, Institute for Advanced Biosciences 38 000 Grenoble, France

[2] Université Claude Bernard Lyon 1, CNRS UAR3444, Inserm US8, ENS de Lyon, SFR Biosciences, Lyon 69007, France

[3]Université Claude Bernard Lyon 1 - Laboratoire de Biologie Tissulaire et d'Ingénierie Thérapeutique, UMR 5305, Université Lyon 1, CNRS, IBCP, Lyon, France

[4] UM de Génétique Chromosomique, Hôpital Couple-Enfant, CHU Grenoble Alpes, Grenoble, France.

[5] UM GI-DPI, CHU Grenoble Alpes, Grenoble, France.

[6] University Grenoble Alpes, INSERM U1209, CNRS UMR5309, Optical microscopy and cell imaging (MicroCell) facility, Institute for Advanced Biosciences, 38000 Grenoble, France

[7] Université Grenoble Alpes, Inserm U1209, CNRS UMR 5309, plateforme Optimal, Institute for Advanced Biosciences 38 000 Grenoble, France

* To whom correspondence should be addressed: Jessica Escoffier, Team "Genetics, Epigenetics and Therapies of Infertility", Institute for Advanced Biosciences (IAB), INSERM 1209, CNRS UMR 5309 University Grenoble Alpes, Grenoble, FRANCE.
Contact:mail to jessica.escoffier@univ-grenoble-alpes.fr
tel: 33 (0)4 76 63 71 11

Ethics statement

All procedures involving animals were performed in line with the French guidelines for the use of live animals in scientific investigations. The study protocol was approved by the local

ethics committee (ComEth Grenoble # 318) and received governmental authorization (ministerial agreement # 38109-2022072716142778).

Abstract

Oligo-astheno-teratozoospermia (OAT), a recurent cause of male infertility, is the most frequent disorder of spermatogenesis with a probable genetic cause. Patients and mice bearing mutations in the *ARMC2* gene have a decreased sperm concentration, and individual sperm show multiple morphological defects and a lack of motility – a canonical OAT phenotype. Intracytoplasmic sperm injection (ICSI) is required to treat such a condition but it is associated with a small increase in birth defects in comparison to pregnancies not involving assisted conception . Consequently, new targeted treatments are needed to restore fertility. Here, a combination of *in vivo* injection and electroporation of capped and poly-A-tailed naked mRNA is tested as a strategy to treat *ARMC2*-related infertility in mouse. mRNAs coding for several reporter genes are tested and the efficiency and the kinetic of expression are assessed using *in vivo* and *in vitro* 2D and 3D imaging experiments. We show that mRNA-coded reporter proteins are detected for up to 3 weeks in germ cells, making the use of mRNA possible to treat infertility. We compare these results with those obtained with a non-integrative plasmid Enhanced Episomal Vector (EEV), which induces low and transient expression in spermatogenic cells. Consequently, injection and electroporation of naked mRNA-*Armc2* into the testes of *Armc2*-deficient males were performed and we show the presence of normal and motile sperm in the epididymis. These motile sperm were able to produce embryos by IVF and ICSI. This study shows for the first time that mRNA-*Armc2* efficiently restores fertility and opens new paths for male infertility treatment.

Key words: Sperm cells, infertility, protein therapy, mRNA, EEV, *In Vivo* Microinjection and Electroporation, *in vivo* imaging, Whole Testis Optical clearing, lightsheet microscopy.

60 **Introduction**

61 Worldwide, 10-15 % of couples (or 70 million) face infertility [1]. Infertility is thus a major
62 public health issue presenting significant medical, scientific and economic challenges (a
63 multibillion € annual market)[2]. A significant proportion of infertilities is due to altered
64 gametogenesis, where the sperm and eggs produced are incompatible with fertilization
65 and/or embryonic development [3]. Approximately 40 % of cases of infertilities involve a male
66 factor, either exclusively, or associated with a female deficiency [4].

67 Male gametogenesis, or spermatogenesis, is a highly complex physiological process which can
68 be split into three successive steps: proliferation (mitosis of spermatogonia), reduction of the
69 number of chromosomes (meiosis of spermatocytes), and morphogenesis of spermatozoa
70 (spermiogenesis). The whole process involves around two thousand of genes, 60 % of which
71 are expressed exclusively in the testes [5]. Because of this multiplicity of genes,
72 spermatogenesis is strongly affected by genetic factors [5], with most severe disorders likely
73 to be of genetic origin.

74 Among infertility disorders, oligo-astheno-teratozoospermia (OAT) is the most frequent (50
75 % [6]) and it is likely to be of genetic origin. Spermatocytograms of OAT patients show a
76 decrease in sperm concentration, multiple morphological defects and defective motility [7, 8].
77 Because of these combined defects, patients are infertile and can only conceive by
78 intracytoplasmic sperm injection (ICSI).

79 ICSI can efficiently overcome the problems faced. Nevertheless, concerns persist regarding
80 the potential risks associated with this technique, including blastogenesis defect,
81 cardiovascular defect, gastrointestinal defect, musculoskeletal defect, orofacial defect,
82 leukemia, central nervous system tumors, and solid tumors [9-12]. Statistical analyses of birth
83 records have demonstrated an elevated risk of birth defects, with a 30-40 % increased
84 likelihood in cases involving ICSI [9-12], and a prevalence of birth defects between 1 % and 4
85 % [11]. To overcome these drawbacks, a number of experimental strategies have been
86 proposed to bypass ARTs and restore spermatogenesis and fertility, including gene therapy
87 [13-16].

88 Gene therapy consists of introducing a DNA sequence into the genome to compensate for a
89 defective gene. It can thus rescue production of a missing protein, and is now applied both in
90 research [17] and for the treatment of human diseases [18] .

91 Given the genetic basis of male infertility, the first strategy, tested in mice, was to overcome
92 spermatogenic failure associated with monogenic diseases by delivery of an intact gene to
93 deficient germ cells [13]. Gene therapy is effective in germ cells, as numerous publications
94 have shown that conventional plasmids can be transferred into spermatogonia in several
95 species with success, allowing their transcription in all cells of the germinal lineage [13-16].
96 Most experiments were performed in mouse models, delivering DNA constructs into living
97 mouse germ cells by testis electroporation after microinjection of a DNA-containing solution
98 into the seminiferous tubules. Using this method, it was possible to rescue meiosis and fertility
99 in mouse models of infertility [13, 16]. However, the genetic changes induced are transmitted
100 to any descendants. Consequently, gene therapy cannot be used to treat infertility in humans,
101 both for ethical reasons and to avoid any eugenic deviations, and currently transmissible
102 changes in humans are illegal in 39 countries [19]. Furthermore, the genetic modification of
103 germ cell lines poses biological risks, including the induction of cancer, off-target effects, and
104 cell mosaicism. Errors in editing may have adverse effects on future generations. It is
105 exceedingly challenging to anticipate the consequences of genetic mosaicism, for instance, in
106 a single individual [20, 21]. Gene therapies have thus raised both ethical controversy and long-
107 term safety issues.

108 For these reasons, we decided to test an alternative strategy to DNA transfection based on
109 the use of naked mRNA. Thanks to this change, the risk of genomic insertion is avoided, and
110 thus there is no question of heritable alterations [22].The first part of this study presents a
111 characterization of the protein expression patterns obtained following transfection of naked
112 mRNA coding for reporter genes into the testes of mice. The second part is to apply the
113 protocol to a preclinical mouse model of OAT. Patients and mice carrying mutations in the
114 *ARMC2* gene present a canonical OAT phenotype and are infertile. The preclinical *Armc2*
115 deficient (*Armc2* KO) mouse model is therefore a valuable model to assess whether *in vivo*
116 injection of naked mRNA combined with electroporation can restore spermatogenesis. We
117 chose this model for several reasons: first, *Armc2* KO mice are sterile and all sperm exhibit
118 short, thick or coiled flagella [13]. As a result, 100 % of sperm are immobile, thus it should be

119 easy to determine the efficacy of the technique by measuring sperm motility with a CASA
120 system. Second, the *Armc2* gene codes for an 867-amino acid protein and this large size
121 represents a challenge for expression in the testis following electroporation.

122 To determine the efficacy of naked mRNA transfection as a method to achieve protein
123 expression in the testes, we first assessed the level of transcription of reporter proteins after
124 mRNA injection compared to the injection of a non-integrating plasmid, the Enhanced
125 Episomal Vector (EEV). EEV is a vector derived from Epstein-Barr virus, it includes an origin of
126 replication (EBV Ori) and the EBNA1 protein. Both elements, allows the synchronous initiation
127 of extra-chromosomal EEV replication with host DNA at each S phase of the cell cycle and the
128 segregation of the EEV episome in daughter cells. It is notable that EEV is maintained at a rate
129 of 90-95% per cell division. It does not integrate or modify the host genome [11, 12].

130 In the present *in vivo* work, we injected and electroporated three distinct mRNAs coding for
131 the following reporter proteins: green fluorescent protein (GFP), luciferase (Luc) and mCherry,
132 and an EEV episome vector containing the sequences coding for both GFP and luciferase
133 reporter proteins. The initial step was to characterize and validate the method of injection in
134 adult males. Subsequently, the kinetics and patterns of expression of the electroporated
135 mRNAs and EEV were compared using a variety of methods, including whole testis imaging, *in*
136 *vivo* bioluminescence imaging, and tissue clearing. Subsequently, the mRNA transfection
137 protocol was tested in a preclinical mouse model of OAT with the objective of restoring
138 fertility.

139

140 **Materials and methods**

141 **Animals**

142 All procedures involving animals were performed in line with the French guidelines for the use
143 of live animals in scientific investigations. The study protocol was approved by the local ethics
144 committee (ComEth Grenoble # 318) and received governmental authorization (ministerial
145 agreement # 38109-2022072716142778).

146 The animals used were (a) B6D2 F1 hybrid (♀ C57BL/6JRj crossed with ♂ DBA/2, Janvier
147 laboratories; France) adult male mice aged between 8 and 25 weeks, (b) the *Armc2* KO mouse

148 strain obtained by CRISPR-Cas9 [23] and (c) CD1 female 6 weeks old (Janvier laboratories, Le
149 Genest-Saint-Isle ,France). Experiments were carried out on wild type (WT) or *Armc2* KO adult
150 male mice aged between 8 and 15 weeks.

151 **Chemicals and reagents**

152 Fast Green (FG) (F7258 – 25 g), phosphate buffered saline (PBS, D853 7-500 mL), hematoxylin
153 (GH5316 – 500 mL), eosin (HT110216 – 500 mL), tert-Butanol (471712 – 100 mL), Histodenz
154 (D2158 – 100 g), sorbitol (S1876 – 100 g), urea (U5128 – 500 g), Potassium Phosphate,
155 Monobasic (P0662), Magnesium Sulfate (anhydrous) (M9397), Sodium Bicarbonate Calcium
156 Chloride · 2H2O (22317), EDTA (E9884), Sodium Lactate (60 % syrup - d= 1,32 g L^{-1}) (L7900),
157 Glucose (G8270), Penicillin (P4333), Streptomycin (P4333), HEPES (H0887), PVA 30,000-70,000
158 (P8136), Albumin, Bovine Fraction V (A3803), M2 medium (M7167), Hyaluronidase (H3884),
159 mineral oil (M8410), PolyVinylPyrolidone (PVP360-100G), M16 medium (MR-016) and
160 Collagenase (C8176) were purchased from Sigma Aldrich (Saint-Quentin-Fallavier, France).
161 Sodium Chloride (1112-A) was purchased from Euromedex (Souffelweyersheim, France).
162 Potassium Chloride (26764) L-Glutamine (35050038), Sodium Pyruvate (11360039), NEAA
163 (11140050) and EAA (11130036) were purchased from Life Technologies, (Waltham, MA USA).
164 Schorr staining solution was obtained from Merck (Darmstadt, Germany). Mfel HF (R35895)
165 and RNase-free DNase I (M03035) were obtained from New England Biolabs (Ipswich, MA,
166 USA). Paraformaldehyde (PFA, 15710) was obtained from Electron Microscopy Science
167 (Hatfield, PA, USA). Ketamine and xylazine were obtained from Centravet (Dinan, France).
168 Fluorescent i-particles (NIRFiP-180) were obtained from Adjuvatis (Lyon, France). Script Gurad
169 RNAse CleanCap AG (040N-7113-1), CleanCAp *EGFP*-mRNA (040L-7601-100), T7-FlashScribe
170 kit (C-ASF3507), poly(A) tail (C-PAP5104H) and CleanCap *Luciferase*-mRNA (L-7602-1000) were
171 obtained from Tebubio (Le Perray en Yvelines, France).

172 **Plasmids**

173 All plasmids, EEV *CAGs-GFP-T2A-Luciferase*, (EEV604A-2; System Bioscience, Palo Alto, CA,
174 USA), mCherry plasmid (given by Dr. Conti MD at UCSF, San Francisco, CA, USA) and EEV-
175 *Armc2-GFP* plasmid (CUSTOM-S017188-R2-3, Trilink, San Diego, CA, USA) were amplified by
176 bacterial transformation (E. coli, EC0112; Thermo Fisher, Courtaboeuf, France). After
177 expansion, plasmids were purified with a NucleoBond Xtra Midi kit (740410-50; Macherey-

178 Nagel, Düren, Germany) using manufacturer's protocol. All plasmids DNA pellets were
179 solubilized in (DNAse- and RNAse-free) milliQ water (Sigma Aldrich, Saint-Quentin-Fallavier,
180 France), before being used.

181 The EEV *CAGs-GFP-T2A-Luciferase* episome contains the cDNA sequences of Green
182 Fluorescent Protein (GFP) and luciferase, under the control of a CAGs promoter (Supp Fig 1).
183 After purification, the EEV *CAGs-GFP-T2A-Luciferase* plasmid concentration was adjusted to
184 9 µg μL^{-1}. Prior to injection, 3.3 µL of this plasmid solution was mixed with 1 µL 0.5 % Fast
185 Green and 5.7 µL sterile PBS to obtain a final EEV concentration of 3 µg μL^{-1}. The EEV-*Armc2-*
186 *GFP* plasmid contains the mouse cDNA sequences of *Armc2 (ENSMUST00000095729.11)* and the
187 Green Fluorescent Protein (GFP) genes under the control of a strong CAGs promoter (Supp Fig
188 1). After amplification and purification, the final plasmid concentration was adjusted to 9 µg
189 μL^{-1} in water. Prior to injection, 3.3 µL of this plasmid solution was mixed with 1 µL of 0.5 %
190 Fast Green and 5.7 µL of sterile PBS to obtain a final EEV concentration of 3 µg μL^{-1}. The
191 *mCherry* plasmid contains the cDNA sequence of *mCherry* under the control of CMV and T7
192 promoters (Supp Fig 1). After amplification and purification, the final plasmid concentration
193 was adjusted to 9 µg μL^{-1}.

194 ***Armc2*-mRNA**

195 *Armc2*-mRNA used for *in vivo* testes microinjection and electroporation was obtained from
196 Trilink (San Diego, CA, USA). The commercial *Armc2*-mRNA has an AG CleanCap, a poly (A) tail
197 of 120 adenosines and 3 HA-FLAG. The main challenge with mRNA-based therapy is mRNA
198 stability. To improve mRNA stability *in vivo* and avoid its degradation by ribonucleases,
199 optimization techniques were implemented. Thus, the used mRNA has codon optimization, a
200 poly (A) tail and a CleanCap. To verify the efficiency of cell transfection, an *EGFP*-mRNA was
201 injected together with the *Armc2*-mRNA. During the injection, the concentration of *EGFP*-
202 mRNA and *Armc2*-mRNA were 300 ng μL^{-1} each.

203 ***mCherry*-mRNA transcription *in vitro***

204 The circular *mCherry* plasmid was linearized using the restriction enzyme MfeI HF at 37 °C for
205 1 h. The pm-*mCherry* was then extracted and purified with the DNA Clean and Concentrator-
206 25 ™ kit (D4033; Zymo Research, Irvine, CA, USA). The pm-*mCherry* was subsequently
207 transcribed in vitro using the T7-FlashScribe kit (C-ASF3507; Tebubio, Le Perray en Yvelines,

208 France). The mRNA was capped with a clean cap (CleanCap AG; 040N-7113-1, Tebubio, Le
209 Perray en Yvelines, France), and a poly(A) tail (C-PAP5104H; Tebubio, Le Perray en Yvelines,
210 France) was added before purification using the NucleoSpin RNA Clean Up kit (740948-50;
211 Macherey-Nagel, Düren, Germany). Prior to injection, *mCherry*-mRNA was mixed with Fast
212 Green to obtain a final concentration of 300 ng μL^{-1} (0.05 % FG, PBS).

213 **Agarose gel electrophoresis of the Episomal Vector EEV and mRNA-mCherry**

214 Before loading on a pre-stained (Gel Green) 1.5 % agarose gel, the EEV-plasmid and mRNA
215 were mixed with a loading dye (Promega Blue Orange G1904, Promega, Charbonnières
216 France). An aliquot of each sample (500 ng) was loaded into each well and electrophoresis was
217 performed for 30 min at 100 V at room temperature (RT). A DNA size marker (Gene ruler
218 SM1331, Thermo Scientific, Courtaboeuf, France) was used to assess molecular weight. Gel
219 images were acquired using a ChemiDoc XRS+ (BIORAD, Marnes-la-Coquette, France).

220 ***In vivo* microinjection and electroporation of testes**

221 Electroporation was conducted as previously described [15]. Briefly, male mice B6D2, *Armc2*$^{+/+}$
222 or *Armc2*$^{-/-}$, depending on the experimental conditions, were anesthetized with
223 ketamine/xylazine solution (100 mg μL^{-1} and 10 mg μL^{-1} respectively). The testes were pulled
224 out of the abdominal cavity or scrotum. Under a binocular microscope and using
225 microcapillaries pipettes (FemtoTip II ®, Eppendorf, Montesson, France), 10 µL DNA (3 µg μL^{-}
226 ^{1} - 0.05 % FG) or mRNA (300 ng μL^{-1} -0.05 % FG) was injected into the seminiferous tubules
227 through the *rete testis* applying a constant pressure (microinjector, Femto Jet 4i, Eppendorf,
228 Montesson, France). Two series of 8 square electric pulses (25 V for 50 ms) were applied to
229 the testis using tweezer-type electrodes linked to an electroporator (Gemini, BTX, Holliston,
230 MA, USA). The testes were then replaced in the abdominal cavity, and the abdominal wall and
231 skin were sutured. For each animal, the left testis was injected and electroporated with the
232 different nucleic acids (mRNA, EEV), whereas the right testis was injected with a control
233 solution (PBS, 0.5 % FG) as a control. Both testes were electroporated.

234 **Flash Freezing and Fluorescence Analysis of testes**

235 Depending on the experimental condition, 1-, 3- or 7-days post injection, the testes were
236 collected and washed for 5 min in PBS. Then, they were embedded in Peel-A-Way Cryomolds

237 filled with OCT Mounting media (VWR, Rosny-sous-Bois, France). The samples were flash
238 frozen in a 100 % isopentane solution (524391; Carlo ERBA, Val-de-Reuil, France), pre-cooled
239 with liquid nitrogen. Once frozen, they were cut into 20 µm sections using a cryostat. The
240 cryostat sections were then fixed with 4 % PFA-PBS for 10 min at 4 °C and counterstained with
241 1.8 µM DAPI (nuclear stain) before observation using an Axioscan Z1 slide scanner or a
242 confocal microscope LSM710 (NLO – LIVE7 – Confocor 3). The fluorescence of the different
243 reporter proteins was detected using appropriate filters for DAPI, GFP, Texas Red (for
244 mCherry), and Cy7 (for the Fluorescent i-particles NIRFiP-180).

245 **Tissue collection and histological analysis**

246 For histological analysis, treated and control B6D2 testes were fixed by immersion in 4 %
247 paraformaldehyde (PFA) for 14 h. They were then embedded in paraffin before cutting into 5
248 µm sections using a microtome (Leica biosystems, Wetzlar, Germany). After deparaffination,
249 the sections were stained with hematoxylin and eosin. Stained sections were digitized at 20x
250 magnification using an axioscan Z1-slide scanner (Zeiss, Jna, Germany). Spermatogenesis was
251 assessed by measuring the area of seminiferous tubules and the cross sections of round
252 tubules (μm^2) ($n > 35$ tubules per testis section; n=5 testis sections per condition). Statistical
253 significance of differences was determined using a Student's *t*-test.

254 ***Ex vivo* Fluorescence Analysis**

255 To analyze the expression of the reporter proteins GFP and mCherry in seminiferous tubules,
256 whole testes were examined under an inverted microscope (CKX53, Olympus, Shinjuku, Tokyo,
257 Japan). Exogenous fluorescence was detected using filters for GFP and Texas Red.

258 **Harris-Shorr sperm Analysis**

259 Sperm were collected from the caudae epididymides of mice (Control, injected with EEV-*GFP*,
260 *GFP*-mRNA, or *Armc2*-mRNA). They were allowed to swim for 10 min at 37 °C in 1 mL M2
261 media. Sperm were centrifuged at 500 g, washed once with PBS, and fixed 4 %
262 paraformaldehyde in PBS for 1 min at RT. After washing with 1 mL acetate ammonia
263 (100 mM), the sperm suspensions were spotted onto 0.1 % poly L-lysine precoated slides
264 (Thermo Scientific, Courtaboeuf, France) and left to dry. Harris–Schorr staining was then
265 performed according to the WHO protocol [24], and at least 150 sperm were analyzed per
266 animal.

267 **Whole Testis Optical clearing and 3D image reconstructions**

268 Optical clearing (adapted from uDISCO and Fast 3D clear protocols)

269 Adult mice were euthanized by cervical dislocation and then transcardiac perfused with 1X
270 PBS (Sigma Aldrich, Saint-Quentin-Fallavier, France). The testes were extracted and fixed for
271 two days at 4 °C in 4 % PFA (Electron Microscopy Sciences, Hatfield, PA ,USA). Samples were
272 then washed with PBS for at least two days. Mouse testes were subsequently dehydrated in
273 graded series of tert-butanol solutions (Sigma Aldrich, Saint-Quentin-Fallavier, France) at 35 °C
274 as follows: 30 % overnight (O/N), 50 % for 24 h, 70 % for 10 h, 80 % O/N, 90 % for 10 h, 96 %
275 O/N, and 100 % for 10 h. The testes were cleared in clearing solution (96 % Histodenz, 2 %
276 Sorbitol, 20 % Urea) for 2 days. Then, nuclei were stained with 3.6 μM DAPI (20 % DMSO; 2 %
277 Triton, 1 % BSA) for 2 days. Finally, the testes were then conserved in the clearing solution at
278 4°C until observation by microscopy. All these steps were carried out under agitation and
279 protected from light.

280 3D tissue Imaging

281 The optically-cleared mouse testes were imaged on a lightsheet fluorescence microscope
282 (Blaze, Miltenyi Biotec, Germany), using a 4x NA 0.35 MI PLAN objective protected by a dipping
283 cap for organic solvents, with an overall working distance of 15 mm. Acquisitions on the
284 horizontal plane were obtained with a fixed lightsheet thickness of 3.9 µm at both 488 nm and
285 561 nm with no overlap between horizontal planes. Voxel resolution x = 1.21; y = 1.21; z = 2
286 µm. 3D reconstructions were created using Imaris software (Oxford Instruments plc,
287 Abingdon, UK).

288 Cellular image analysis

289 The optically-cleared mouse testes were imaged using a 'ConfoBright' system which is a
290 unique adaptive optics confocal microscope (Nikon A1R MP, Nikon Europe B.V., The
291 Netherlands) equipped with a deformable mirror module (AOS-micro, AlpAO, Montbonnot,
292 France) to correct geometrical aberrations. Indeed, the 3D confocal imaging of cleared sample
293 requires long distance objectives for deep tissue imaging, resulting in optical aberrations due
294 to inhomogeneous refractive index. The 'ConfoBright' microscope corrects these geometric
295 optical aberrations both in excitation and detection light path and restores locally the high

296 diffraction-limited spatial resolution and the best possible photon collection efficiency. The
297 driving metrics based on molecular brightness was used to optimize the adaptive optics in the
298 isoplanatic patch of ca. 100 mm at each imaged depth. Images were acquired using an apo
299 LWD 40x/1.15 water immersion objective (WD 600 µm) and a Plan apo 10x/0.45 objective. FIJI
300 software (open-source software[25]) was used to process and analyze images and Imaris
301 software for the 3D reconstructions.

302 **Bioluminescence imaging**

303 *In vivo* Bioluminescence imaging was performed at several time points after *in vivo Luciferase*
304 -mRNA or EEV-*GFP-luciferase* injection and electroporation (n=5 mice per condition). Ten
305 minutes before imaging, mice received an intraperitoneal injection of 150 µg g^{-1} of D-luciferin
306 (Promega, Charbonnières France), and were then anesthetized (isoflurane 4 % for induction
307 and 1.5 % for maintenance) before placing in the optical imaging system (IVIS Lumina III,
308 PerkinElmer, Courtaboeuf, France). *In vivo* bioluminescence signals were measured in selected
309 regions of interest (injected testes) and were expressed as mean photons per second (mean
310 ± SEM). Background bioluminescence was measured on images from control mice. When the
311 *in vivo* bioluminescence signal was no longer detectable, testes were collected and immersed
312 in a luciferin solution for a few minutes before performing *ex vivo* imaging to confirm the
313 absence of signal.

314 **Sperm motility**

315 The cauda epididymis was dilacerated in 1 mL of M2 medium (Sigma Aldrich, Saint-Quentin-
316 Fallavier, France) and spermatozoa were allowed to swim out for 10 min at 37 °C. After
317 incubation, 30 µl of the sperm suspension was immediately placed onto analysis chamber (2X-
318 CEL Slides, 80 µm depth, Leja Products B.V., The Netherlands) kept to 37°C for microscopic
319 quantitative study of sperm movement. Motility of the spermatozoa was evaluated at 37°C
320 with an Olympus microscope and Computer Aided Sperm Analysis (CASA) (CEROS II apparatus;
321 Hamilton Thorne, Beverley, MA, USA). The settings employed for analysis were: acquisition
322 rate: 60 Hz; number of frames: 30; minimum contrast: 30; minimum cell size: 4; low-size gate:
323 0.13; high-size gate: 2.43; low-intensity gate: 0.10; high-intensity gate: 1.52; minimum
324 elongation gate: 5; maximum elongation gate: 100; magnification factor: 0.81.

325 The motility parameters measured were: straight line velocity (VSL); curvilinear velocity (VCL);
326 averaged path velocity (VAP); amplitude of lateral head displacement (ALH); beat cross

327 frequency (BCF); linearity (LIN); straightness (STR). Hyperactivated sperm were characterized
328 by VCL > 250 µm s^{-1} , VSL > 30 µm s^{-1}, ALH > 10 µm and LIN < 60, Intermediate by VCL >
329 120 µm s^{-1} and ALH > 10 µm, progressive sperm by VAP > 50 µm s^{-1} and STR > 70 % and slow
330 sperm by VAP < 50 µm $s^{-1}$and VSL < 25 µm s^{-1}.

331 **Western blot**

332 Western blotting was performed on HEK-293T cells (ATCC, Manassas, VA, USA) transfected
333 with EEV-*Armc2* or *Armc2*-mRNA. Cells were transfected using JetPrime (101000027; Polyplus
334 Illkirch, France) for DNA and JetMessenger (101000056; Polyplus Illkirch, France) for mRNA
335 vectors, both according to the supplier's recommendations. After 48 h, the cells were washed
336 with PBS and scraped off before centrifuging at 4 °C, 1500 RPM for 5 min. The cell pellet was
337 then resuspended in lysis buffer (87787; Thermo Scientific, Courtaboeuf, France)
338 supplemented with an EDTA-free cocktail of protease inhibitors (11836170001; Roche, Bale,
339 Swiss). The suspension was stirred at 4 °C for 2 h, and then centrifuged at 16,000 g at 4 °C for
340 10 min. The protein content of the supernatant was estimated with QuantiPro™ BCA Assay kit
341 (Sigma Aldrich, Saint-Quentin-Fallavier, France) before adding 5X Laemmli + 5 % β-
342 mercaptoethanol and heating at 95 °C for 10 min. For the Western blot, 30 µg of proteins were
343 deposited on a ready-made Bis-Tris gel 12 % (Thermo Fisher, Courtaboeuf, France). After the
344 transfer, the PVDF membrane was blocked with 5 % milk in Tris-Buffered Saline solution
345 containing 0.1 % Tween 20 (TTBS) before immunodetection. The anti HA antibody
346 (11867423001; Sigma Aldrich, Saint-Quentin-Fallavier, France) was diluted in TTBS at 1/5000.
347 After incubation with secondary antibodies (AP136P; Sigma Aldrich, Saint-Quentin-Fallavier,
348 France) diluted at 1:10,000 in TTBS, binding was revealed with an enhanced
349 chemiluminescence detection kit (1705062; Clarity Max Western ECL Substrate; BIORAD,
350 Marnes-la-Coquette, France). Membranes were imaged on a ChemiDoc™ system (BIORAD,
351 Marnes-la-Coquette, France).

352 **Immunofluorescence**

353 Immunofluorescence analysis of dissociated testicular cells was performed as follows. After
354 collection, the tunica albuginea was removed from the testes. Then the tissue was
355 mechanically separated with 18G needles. Once washed with PBS, the testicular cells were
356 placed in a dissociation medium containing 1 mg collagenase type V /mL RPMI for 20 min at
357 37 °C. After filtration (100 µm filter) and centrifugation (5 min at 200 g) the pellets were

358 resuspended in PBS before centrifugation once again. The pellet was then fixed in 1 mL PFA 4
359 % for 5 min. Then 10 mL of ammonium acetate (0.1 M) was added. Finally, 2 mL of medium
360 was spread on a slide. Testicular cells were permeabilized with 0.1 % PBS-Triton X-100 for
361 20 min at room temperature. Slides were then blocked in 10 % BSA with PBS-Tween 0.1 % for
362 30 min before incubating overnight at 4 °C with primary antibodies anti-rabbit *ARMC2* (1/50)
363 (HPA053696, Sigma Aldrich, Saint-Quentin-Fallavier, France) and anti-guinea pig tubulin
364 (1/100) (AA345, Swiss Institute of Bioinformatics, Lausanne, Swiss) diluted in PBS-Tween 0.1
365 % - 5 % BSA. Slides were washed with PBS before incubating for 1 h with secondary antibodies:
366 anti-guinea pig (1/500) (A-11073, Thermo Fischer, Courtaboeuf, France) and anti-rabbit
367 (1:1000) (A-11036, Thermo Fischer, Courtaboeuf, France). Samples were counterstained with
368 DAPI and mounted with DAKO mounting media (NC2313308; Life Technology, Courtaboeuf,
369 France). Fluorescence images were acquired under a confocal microscope (Zeiss, Jena,
370 Germany) fitted with a 63× oil immersion objective. Images were analyzed with ZEN lite
371 software (Zeiss, Jena, Germany).

372 **Intra-cytoplasmic sperm injection (ICSI)**

373 Collection of gametes for ICSI

374 *Armc2*$^{-/-}$ sperm or *Armc2*$^{-/-}$ rescued sperm were harvested by dilaceration of the cauda
375 epididymis. They were allowed to swim for 10 min at 37°C in 1 ml of CZB.HEPES medium
376 containing (in mM) (HEPES 20, NaCl 81.6, KCl 4.8, $MgSO_4$ 1.2, $CaCl_2$ 1.7, KH_2PO_4 1.2,
377 EDTA.Na_2 0.1, Na-lactate 31, $NaHCO_3$ 5, Na-pyruvate 0.3, polyvinyl alcohol 0.1 mg mL^{-1}, phenol
378 red 10 mg mL^{-1} (0.5 % (w/v) in DPBS), pH 7.4) KCl 125, NaCl 2.6, Na_2HPO_4 7.8, KH_2PO_4 1.4 and
379 EDTA 3 (pH 7.0)).The sperm head was separated from the tail by applying multiple piezo pulses
380 (PiezoXpert®, Eppendorf, Montesson, France)

381 Eggs preparation

382 CD1 female mice, 7 weeks old, were superovulated by IP injection of 7.5 IU pregnant mare's
383 serum gonadotrophin (PMSG; Centravet, Dinan, France) followed by 7.5 IU HCG (Centravet,
384 Dinan, France) 48 h later. Eggs were collected from oviducts about 14 h after HCG injection.
385 Cumulus cells were removed with 0.1 % hyaluronidase in M2 medium for 5–10 min. Eggs were
386 rinsed thoroughly and kept in KSOM medium containing (in g L^{-1}: NaCl 5.55, KCl 0.19,
387 KH_2PO_4 0.05, $MgSO_4$ 0.05, $NaHCO_3$ 2.1, $CaCl_2 \cdot 2H2O$ 0.250, EDTA 0.004, L-Glutamine 0.146,

388 Na-lactate 1.870, Na-pyruvate 0.020, Glucose 0.04, Penicillin 0.05, Streptomycin 0.07, BSA
389 1.000, NEAA 0.5 % and EAA 1 %.), at 15°C for at least 15 min until required for ICSI.

390 ICSI procedures

391 ICSI was performed according to the method described by Yoshida and Perry (2007)[26].For
392 microinjection, *Armc2*$^{-/-}$ sperm or *Armc2*$^{-/-}$ -rescued motile sperm heads were separated from
393 the tail by applying multiple piezo pulses (PiezoXpert®, Eppendorf, Montesson, France). Sperm
394 heads were introduced into the ooplasm using micromanipulators (Micromanipulator
395 InjectMan®, Eppendorf, Montesson, France) mounted on an inverted Nikon TMD microscope
396 (Nikon, Minato-ku, Tokyo, Japan). Eggs that survived the ICSI procedure were incubated in
397 KSOM medium at 37 °C under in an atmosphere of 5 % CO_2. Pronucleus formation was checked
398 at 6 h after ICSI, and outcomes were scored up to the blastocyst stage.

399 ***In vitro fertilization (IVF).***

400 *Armc2*$^{-/-}$ sperm or *Armc2*$^{-/-}$ rescued sperm were harvested by dilaceration of the cauda
401 epididymis. They were allowed to swim in *IVF* well in capacitated media (M16 + 4 % BSA) at
402 37 °C for 10 minutes. Eggs were collected from mature CD1 females (6 weeks old)
403 synchronized with 7.5 units of pregnant mare serum gonadotrophin (PMSG) and 7.5 units of
404 human chorionic gonadotrophin (hCG) prior to collection. Cumulus were incubated for 10
405 minutes in 500 µL M16 (MR-016; Sigma Aldrich, Saint-Quentin-Fallavier, France) / 1mg L^{-1}
406 collagenase (C8176, Sigma Aldrich). Cumulus-free and zona-free eggs were collected, and
407 rinsed twice with 500 µl M16 medium. Eggs were incubated with either *Armc2*$^{-/-}$ sperm or
408 *Armc2*$^{-/-}$ rescued sperm) in capacitated medium (37 °C, 5 % CO_2) for 4 hours. After incubation,
409 unbound sperm were washed away and eggs were incubated with KSOM at 37 °C, 5 % CO_2.
410 Twenty-four hours after fertilization, we scored the different stages (unfertilized oocytes,
411 aborted embryos, and 2-cell embryos as an indication of successful fertilization).

412 **Statistical analyses**

413 Statistical analyses were performed using SigmaPlot (version 10; Systat Software, Inc., San
414 Jose, CA, USA). To account for sample variability between animals, a paired t-test, Mann-
415 whitney rank sum test, on-way Anova and Wilcoxon test were used. Data are displayed as
416 mean ± SEM. P values of * ≤ 0.05, ** ≤ 0.01, or *** ≤ 0.001 were considered to represent
417 statistically significant differences.

418 **Results**

419 **1. *In vivo* microinjection and electroporation of mouse testes**

420 Two routes have been described for microinjection of DNA into the testes: direct injection
421 through the *tunica albuginea,* or injection into the lumen of the seminiferous tubules via the
422 *rete testis*. We chose the *rete testis* route and evaluated the efficacy of the microinjection
423 protocol. In particular, we wished to better characterize the diffusion of the injected solution
424 in the volume of the testis, as we were unable to find any information on this parameter in
425 the literature. The efficacy of microinjection *via rete testis* was assessed using fluorescent i-
426 particles NIRFiP-180, and by measuring their diffusion in testis cross sections examined by
427 microscopy 3 days post-injection (Fig 1). To avoid lesions due to overfilling, the injection was
428 controlled by measuring the expansion of the staining of the peripheral seminiferous tubules
429 during the injection. Injections were stopped when the testes were filled to 2/3 of their
430 capacity (Fig 1A-B). In testis cross sections, the fluorescent i-particles NIRFiP-180 were
431 heterogeneously distributed, and mainly observed in seminiferous tubules located in the
432 peripheral region of the testes, with fewer particles present in the center of the testes (Fig 1C-
433 D). Moreover, no fluorescent i-particles NIRFiP-180 were visible in the peritubular space.
434 These results indicated that microinjection through the *rete testis* did not produce a
435 homogenous distribution of the particles throughout the seminiferous tubules. Nevertheless,
436 the seminiferous tubules remained intact, as no signal was observed in the peritubular space
437 (Fig 1C-D).

438 Next, we assessed the overall safety of the *rete testis* microinjection and electroporation of
439 mRNA and EEV into testes. The safety of the protocol was evaluated by comparing
440 macroscopic and microscopic anatomies of control (injected with control solution, PBS, 0.05
441 % FG), and treated testes (injected either with EEV-*GFP* (PBS, 0.05 % FG) or *GFP*-mRNA (PBS,
442 0.05 % FG)). Three days post-injection, the testes were first observed under a binocular
443 microscope to identify possible macroscopic degeneration of the seminiferous tubules (Fig 2
444 A1 and 2 B1). Degenerations appears as pearly white lesions at the surface of the testis as
445 illustrated in Supp Fig 2 following over electroporation. With the protocol we have developed,
446 no such lesions were observed. Next, the testes were measured and weighed. No statistical
447 differences in length and weight were observed between control and treated testes (Fig 2 A2,
448 A3, B2, B3). Then, microscopic differences were sought by histological analysis of 5 µm

449 sections (Fig 2C). No difference was observed between the control condition and EEV-*GFP* or
450 *GFP*-mRNA on the full cross sections (Fig 2 C1, C2, C3). Next, we observed all the different
451 testicular cells, including all germ cell types and Sertoli cells (Fig 2 D1, D2, D3) for each
452 condition. The layered structure of germ cells was identical in all conditions. Analysis of the
453 histological sections revealed no differences in the tubules area of the testes injected either
454 with EEV-*GFP* or *GFP*-mRNA (Fig 2 E). At last, Harris-Shorr staining of the epididymal sperm
455 cells demonstrated that there were no increases in morphological defects when mRNA and
456 EEV were used in comparison with the control (Fig 2 F4). Taken together, these results suggest
457 that *in vivo* microinjection and electroporation of EEV or mRNA did not perturb
458 spermatogenesis.

459 **2. Analysis of EEV-*GFP* and *GFP*-mRNA testicular expression by whole testis imaging**

460 After validating the injection method, we compared the kinetics of GFP expression and the
461 maintenance of the fluorescent signals for mRNA and EEV. To do so, we injected and
462 electroporated one testis of adult B6D2 mice with EEV-*GFP* (n=129) or with *GFP*-mRNA (n=65).
463 At 0-, 1-, 7-, 15-, 21-, 28-, 35-, 42- and 49-days post-injection, the whole testes were observed
464 under an inverted microscope. The exogenous fluorescence was directly visible at the surface
465 of the testes when illuminated with light at the appropriate wavelength (Fig 3 and Fig 4). No
466 testicular lesions were observed on the testes at any post injection time (Fig 3 A1-H1 and Fig
467 4 A1-F1). In addition, both *GFP*-mRNA and EEV-*GFP* induced GFP expression in the testes (Fig
468 3 A2-H2 and Fig 4 A2-F2). It is worth noting that both vectors induced GFP expression at one
469 day post-injection. However, the duration of fluorescent signals were different. For EEV, GFP
470 fluorescence was still observable on day 42 for 100 % of samples, and 56 % of samples were
471 positive on day 49, indicating that expression lasted around 1.5 months (Fig 4G). In contrast,
472 for mRNA, 100 % of testes were labeled on day 21, but none showed any fluorescence on day
473 28 (Fig 4G). Thus, EEV transfection allowed a considerably longer duration of expression than
474 mRNA. (Fig 3 and 4). It is important to underline that the signal measured is the fluorescence
475 emitted by the GFP. This signal is dependent on both the half-lives of the plasmid/mRNA and
476 the GFP. Therefore, the kinetic of the signal persistence (which is called here expression) is a
477 combination of the persistence of the vector and the synthesized protein. In addition to
478 differences in duration of expression, the GFP expression patterns were clearly different:
479 mRNA produced a large, diffuse pattern, highlighting the shape of the seminiferous tubules;

480 EEV-*GFP* produced a punctiform pattern (Fig 3B and 4B.) These results suggest that *GFP*-mRNA
481 and EEV-*GFP* targeted different seminiferous cell types, such as Sertoli cells and all germline
482 cells, or that there were differences in terms of transfection efficiency.

483 ***3.* Kinetics of EEV and mRNA expression assessed by *in vivo* imaging.**

484 To further assess and compare the kinetics of the expression of the two vectors, we expressed
485 exogenous luciferase in the testis using EEV or mRNA and observed the level of luciferase by
486 *in vivo* bioluminescence imaging. For EEV, we took advantage of the fact that the EEV plasmid
487 contains the DNA sequence of the luciferase protein (*CAGs-GFP-T2A-Luciferase*) in addition to
488 the DNA sequence of the GFP fluorescent protein (Supp Fig 1). For mRNA, we injected
489 commercial naked *luciferase*-mRNA into the *rete testis* according to the same protocol as used
490 for *GFP*-mRNA. For this set of experiments, we injected the EEV-*GFP-Luc* and *luciferase*-mRNA
491 into the testes of 6 adult mice on day 0. We injected a similar number of copies of mRNA and
492 EEV. The testes were imaged *in vivo* to detect bioluminescence expression, on day 1 and
493 weekly until disappearance of the signal, no more than 120 days post-injection (Fig 5). For
494 EEV-*GFP-Luciferase*, the bioluminescence induced by transfection was detected from day 1.
495 After a rapid decrease in signal intensity over the first 3 weeks, a weak but constant signal
496 remained detectable for 3 months, then faded away (Fig 5 A1-A2). For *Luciferase*-mRNA,
497 expression was also detected from day 1. The bioluminescence decreased gradually over 3
498 weeks, becoming undetectable thereafter (Fig 5B1-B2). These results are consistent with our
499 previous results (Fig 3) and confirm that EEV allows a longer expression of exogenous protein
500 within the testis. Fig 5C compare the kinetics of expression observed with EEV and mRNA.
501 Overall, our results indicated a stronger expression for mRNA than for EEV, but with
502 expression decreasing rapidly over-time, and almost no remaining signal after 3 weeks. In
503 contrast, residual expression was detectable for several months with EEV.

504 **4. Assessing testicular and cellular *GFP*-mRNA expression using whole testicle optical**
505 **clearing, lightsheet microscopy, and 3D reconstructions**

506 To better characterize the spatial distribution of *GFP*-mRNA expression in the testis, we
507 performed whole testicular optical clearing. On day 0, we injected and electroporated testes
508 with *GFP*-mRNA (n=6). On day 1, we harvested the testes and cleared them with a modified
509 optical clearing protocol, as described in the MM section. After complete clearing (Fig 6 A), we

510 imaged the whole testes using a lightsheet microscope and performed 3D reconstruction from
511 the images stack obtained (videos 1, 2 and Fig 6 B). From this 3D reconstruction, we
512 determined the volume of the testis stained with GFP by measuring the GFP-positive area in
513 each image and multiplying it by the thickness of the z-step (10 µm). Due to optical issues,
514 only half part of the whole testis was acquired, then the sample was turned by 180 ° to acquire
515 the other half part. A total GFP-stained volume of 0.51 mm^3 and 0.23 mm^3 was determined
516 from the face A and the face B, respectively. The corresponding total volume of half part of
517 the testis was measured as 60 mm^3, therefore 0.81 % and 0.24 % of the testis was transfected
518 for the face A and the face B, respectively (Fig 6 B).

519 **5. Assessing GFP cellular expression using whole testicle optical clearing and adaptive**
520 **optics confocal microscopy**

521 Because the GFP fluorescence patterns were different for the two nucleic vectors when
522 observed under the inverted microscope (Fig 3), we wondered whether the same cell types
523 were targeted in both cases. To address this question, the whole optical cleared testes from
524 EEV-*GFP* and *GFP*-mRNA-transfected mice were imaged using a confocal microscope. The
525 different cell types were identified based on their positions within the seminiferous tubule,
526 their cellular shape and their nuclear morphology - revealed by nuclear staining. For instance,
527 Sertoli cells have an oval to elongated nucleus and the cytoplasm presents a complex shape
528 ("tombstone" pattern) along the basement membrane [27]. Round spermatids have small,
529 round and compact nuclei with a nucleolus and are localized between the spermatocytes and
530 elongated spermatids [28]. For EEV-*GFP*, on day 1 post injection and electroporation, a strong
531 punctiform green fluorescence was visible inside the seminiferous tubules (Fig 7 A). Based on
532 the different morphological criteria, this fluorescent signal was detected in spermatocytes,
533 round spermatids and Sertoli cells (Fig 7 BC). On day 7, the GFP signal induced by EEV-*GFP* was
534 reduced and only isolated signals in a few seminiferous tubules (1 per 11 tubules) were
535 observed (Fig 7 D). These signals were associated only with Sertoli cells only (Fig 7 E).

536 For the mRNA vector, on day 1 and day 7 post-injection and electroporation, an intense
537 fluorescence was observed in all the germ cells and in Sertoli cells in the seminiferous tubules
538 (Fig 8A). At the cellular level, this fluorescent signal was associated with spermatogonia,
539 spermatocytes, round spermatids, elongated spermatids, and mature spermatids cells to
540 similar extents for both post-injection times (Fig 8 B, D). In contrast to what was observed with

541 EEV on day 7, no reduction in the number of fluorescent seminiferous tubules was noted when
542 using *GFP*-mRNA, with 8 out of 10 tubules stained (Fig 8 CD).

543 **6. Expression of naked *mCherry*-mRNA in testis following electroporation**

544 Heterologous expression is well known to depend on the protein studied, we therefore tested
545 the same reporter proteins to compare the mRNA and EEV vectors in the experiments
546 presented above. Apart from the bioluminescence experiments with luciferase, we compared
547 only GFP protein expression. To validate and confirm the capacity of naked mRNA to express
548 proteins in the testes after injection and electroporation, we further challenged the method
549 with mCherry, another reporter protein (Supp Fig 1BD). We injected homemade naked mRNA
550 coding for mCherry into the testes. As previously with *GFP*-mRNA, no testicular lesions were
551 observed (Supp Fig 3 A1, B1, C1, D1, E1, F1).

552 The assessment of the temporal persistence of testicular mCherry fluorescent protein
553 expression revealed a robust red fluorescence from day 1 post-injection, which remained
554 detectable for at least 15 days (Supp Fig 3 B2, C2, and D2). At the cellular level, the fluorescent
555 signal was detected in germ cells, including spermatogonia, spermatocytes, round spermatids,
556 mature spermatids, and Sertoli cells on days 1 and 7 post-injection (Supp Fig 4).

557 Finally, we compared the kinetics and levels of expression of the three different mRNA
558 molecules, coding for mCherry, GFP and luciferase. By comparing the number of mice
559 expressing *mCherry*-mRNA, *GFP*-mRNA and *luciferase*-mRNA fluorescence/luminescence over
560 21 days, we observed first that expression was detectable for all mRNAs on day 1, and second
561 that the duration of expression was slightly different for the individual mRNAs. For instance,
562 on day 15, 100 %, 80 % and 60 % of mice injected with *GFP*-mRNA, *mCherry*-mRNA, and mRNA-
563 *luciferase*, respectively presented fluorescence/bioluminescence and on day 21, 100 % of mice
564 expressed GFP, whereas no signal was observed for mCherry or Luciferase (Supp Fig 5).

565 **7. Endogenous expression of ARMC2 in germ cells**

566 Before attempting to rescue expression, we felt it was important to better characterize *Armc2*
567 expression in healthy germ cells, and in particular to study the timing of expression.

568

569 IF was used to determine when ARMC2 protein was detectable during spermatogenesis. For
570 these experiments, dissociated cells from testes were observed to detect the presence of
571 ARMC2 on different spermatogenic cells. ARMC2 was present only in the flagella of the
572 elongated spermatids (Fig 9A and Supp Fig 6A). The specificity of the signal was validated using
573 testicular cells from Armc2 KO mice, where no signal was observed on all spermatogenic cells
574 (Fig. 9B). In transversal sections of WT seminiferous tubules, ARMC2 signal was not present in
575 spermatogonia and spermatocytes (Supp Fig 6B), but detected in spermatid layers.

576 By analyzing the RNA-seq database produced by Gan's team [29], we show that the mRNA
577 encoding ARMC2 starts to be expressed at the pachytene spermatocyte stage, then shows a
578 gradual increase at the round spermatid stage, and finally becomes predominantly expressed
579 at the elongated spermatid stage (Supp Fig 6C), a result in agreement with a post-meiotic
580 function of the protein. Finally, we also consistently observed a staining at the base of the
581 manchette of elongating spermatids but we have no explanation for that (Fig 9A3).

582 In conclusion, the results presented here demonstrate that the ARMC2 protein is expressed
583 and translated at the late stages of spermatogenesis.

584 **8. Co-injection of *Armc2*-mRNA and *eGFP*-mRNA followed by electroporation is safe**
585 **and induces green fluorescence in the seminiferous tubules.**

586 We next tested whether the injection and electroporation of *Armc2*-mRNA molecules had any
587 deleterious effects on testis anatomy and seminiferous tubule structure. We first verified the
588 quality of *Armc2*-mRNA synthesis by transfecting HEK cells and performing Western blot (Supp
589 Fig 7). After this validation, we co-injected *Armc2*-mRNA and *eGFP*-mRNA into the left testes
590 of mice, using the right testes as untreated controls. *eGFP*-mRNA was co-injected to verify and
591 monitor transfection efficiency. The testes were observed under a binocular microscope at
592 different times (3-, 6-, 10-, 15-, 21-, 28- and 35-days) after electroporation to identify possible
593 macroscopic degeneration of the seminiferous tubules. No morphological defects were
594 observed in the testes co-injected with *Armc2*-mRNA and *eGFP*-mRNA. An example of control
595 and injected testes from day 15 is presented in Fig 10 A1, B1. The testes were also weighed at
596 different times post-injection, and the weight ratios of injected testes to non-injected control
597 testes were determined. For all-time points, this ratio was close to 1 (Fig 10 C), confirming that
598 the method and the mRNAs did not cause any injury at the organ level. Next, under blue light,

599 the efficiency of the transfection was assessed by observing the GFP fluorescence at the
600 surface of the testes. GFP fluorescence was observed on testes injected with *Armc2*-mRNA
601 and *eGFP*-mRNA 2 weeks after injection (Fig 10 B2), indicating that the naked mRNA was
602 successfully transfected into testicular cells.

603 **9. Motile sperm cells detected in *Armc2* KO mice following *Armc2*-mRNA injection and**
604 **electroporation into testes**

605 We then assessed whether the injection of *Armc2*-mRNA into the testes in *Armc2* KO mice
606 restored sperm motility. We examined motility of sperm cells present in the caudal part of the
607 epididymis at different times post-injection (3- to 35-days post-injection). For each condition,
608 between 3 and 16 KO mice were used.

609 The *Armc2* KO model used is known to produce sperm cells with short and irregular flagella
610 that are therefore immotile on day 0. No motile sperm were observed on days 3, 6, 10, 15 or
611 28 after surgery (Fig 11 A). However, motile sperm cells were found in the epididymis of some
612 *Armc2* KO mice at 21- and 35-days post-treatment (Fig 11 A). Indeed, 1 in 3 mice had motile
613 sperm at 21 days post-surgery, rising to 3 in 4 mice at 35 days post-injection. Nevertheless,
614 the number of motile sperm observed remained low: 5.5 % after 21-days and 7.15 % after 35-
615 days post-injection (Fig 11 A1). The sperm motility parameters of *Armc2*$^{-/-}$-rescued motile
616 sperm were characterized in comparison to those of *Armc2*$^{+/+}$ sperm using the computer-
617 assisted semen analysis (CASA) system (Fig 11 A2). These parameters included VAP, VSL, VCL,
618 ALH, BCF, and STR. We have observed significant differences between WT and rescued sperm.
619 In particular, the VSL and LIN parameters are lower for rescued sperm. Next sperm were
620 sorted as progressive, intermediate, hyperactivated, or slow according to motility parameters
621 of motile sperm and recorded from their track (Figure 11A3). The percentage of
622 hyperactivated sperm and the proportion of intermediates in the *Armc2*$^{-/-}$-rescued motile
623 sperm population were found to be increased in comparison to the control. Videos showing
624 sperm motility in different conditions are available in the online material associated with this
625 article (Videos 3 to 6).

626 After verifying motility, we looked at the morphology of the spermatozoa present in the cauda
627 epididymis. Six days after injection of *Armc2*-mRNA, the cells detected were mostly round cells
628 and abnormal spermatozoa with a short or coiled flagellum measuring between 7 and 20 µm.

629 The same cell types were observed at 3-, 10-, 15- and 28-days post-surgery. In contrast, the
630 motile sperm detected on days 21 and 35, had a normal morphology with a long flagellum
631 (greater than 100 µm) and a hook-shaped head (Fig 11 B and Supp Fig 8).

632 **10. Motile sperm cells detected in *Armc2* KO mice following *Armc2*-mRNA injection and**
633 **electroporation into testes are fertile**

634 We subsequently evaluated the efficacy of *Armc2*-mRNA injection into the testes of *Armc2* KO
635 mice in restoring sperm fertility. The fertility outcome was assessed through *in vitro*
636 *fertilization* (IVF) and intracytoplasmic sperm injection (ICSI) experiments. The sperm rescued
637 from *Armc2*$^{-/-}$ mice were capable of successfully fertilizing eggs and producing embryos at the
638 two-cell stage by IVF (Fig 12 A1-A2). Notably, 62.7% of two-cell embryos were obtained with
639 the *Armc2*$^{-/-}$-rescued sperm by IVF, compared to only 2.67% with the *Armc2*$^{-/-}$ sperm. Three %
640 of eggs became 2-cell embryos when fertilized with sperm from *Armc2*$^{-/-}$, a rate not
641 significantly different to that observed for eggs incubated 24 h without sperm, and likely
642 corresponding to parthenogenesis activation (Fig 12 A1-A2).

643 To gain further insight, a comparative analysis of the developmental outcomes of mouse
644 embryos generated by ICSI with spermatozoa from wild-type (WT), *Armc2*$^{-/-}$ and *Armc2*$^{-/-}$
645 treated mice was performed. It should be noted that in case of *Armc2*$^{-/-}$ treated mice, the ICSI
646 procedure was performed only with the motile *Armc2*$^{-/-}$-rescue spermatozoa. The percentage
647 of live injected oocytes that reached the blastocyst embryos was 46% for WT spermatozoa,
648 25% for *Armc2*$^{-/-}$-rescued spermatozoa and 13% for *Armc2*$^{-/-}$ spermatozoa (Fig. 12B). The
649 findings indicate that the developmental potential of the embryos was enhanced when *Armc2*$^{-}$
650 $^{/-}$-rescued sperm were utilized as opposed to *Armc2*$^{-/-}$ sperm.

651 Overall, these results demonstrate that the *Armc2*$^{-/-}$-rescue motile spermatozoa can
652 successfully fertilize eggs and produce embryos capable of developing properly into
653 blastocysts.

654 **Discussion**

655 The challenge of treating male infertility remains to be addressed. Current assisted
656 reproduction techniques (ARTs) are unable to treat all patients, and alternative strategies
657 need to be developed to meet the legitimate desire to be a father. The aim of this study was
658 to evaluate the potential of naked mRNA as a means to induce an expression of exogenous

659 proteins in male germ cells in a preclinical adult mouse model. Based on previous studies using
660 electroporation, we investigated whether the combination of the injection of naked mRNA
661 and in *vivo* electroporation could lead to an efficient protein expression in spermatogenic
662 cells. We chose to first study the efficiency of capped and poly(A)-tailed mRNA coding for
663 reporter proteins and compared the results to those obtained with a non-integrative
664 enhanced episomal vector plasmid. No EEV plasmid has ever been tested in the context of
665 infertility treatment before this study.

666 Using an adult mouse model, we optimized the micro-injection and electroporation method
667 described by Michaelis et al [15]. We show that the microinjection through the *rete testis* did
668 not provide a homogenous distribution of the particles throughout the seminiferous tubules.
669 Nevertheless, the seminiferous tubules remained intact, with no signal detected in the
670 peritubular space. The peripheral expression observed was due to the close vicinity of cells to
671 the electrodes, and to a peripheral dispersal of the injected solution, as shown by the
672 distribution of the fluorescent i-particles NIRFiP-180. Our results also showed that the
673 combination of injection and electroporation did not perturb spermatogenesis when electric
674 pulses are carefully controlled. Using such a protocol, we were able to induce the expression
675 of 3 reporter proteins, GFP, mCherry and luciferase in the testis by mRNA
676 injection/electroporation.

677 Using whole testicular optical clearing, the reporter proteins were synthesized from the
678 injected mRNA in different types of cells including Sertoli cells, spermatogonia, spermatocytes,
679 round spermatids, and mature spermatids from day 1, and were still detectable after 1 week.
680 These results deserve two comments: first, the expression is very fast and synthesized protein
681 is detectable 24 h injection, second all cell types have the ability to translate mRNAs.
682 Furthermore, the fact that we observed motile sperm at 21 days after injection confirms that
683 spermatids are transfected and that the translation of the protein of interest is possible at this
684 stage. For EEV, we have a similar result at day 1. However, the yields of seminiferous tubules
685 and cellular transfection are lower. In particular, a lower level of transfection of germ cells was
686 observed than with the mRNA. It is worth noting that after one week, the reporter proteins
687 synthesized from injected EEV, were only discernible in the Sertoli cells.

688

689 Based on whole testes fluorescence and, for the first time, *in vivo* bioluminescence imaging of
690 testes, we characterized the kinetics of mRNA expression. The signal measured is the
691 fluorescence or the bioluminescence emitted by the GFP or luciferase. This signal is dependent
692 on both the half-lives of the plasmid/mRNA and the proteins. Therefore, the kinetic of the
693 signal persistence is a combination of the persistence of the vector and the synthesized
694 protein. For mRNA, it's difficult to determine the lifespan of our mRNAs because these mRNAs
695 have been modified at different levels including 5'CAP, mRNA body, poly(A)tail, which increase
696 mRNA stability and translation [30]. Nevertheless, their half-lives should not exceed a few days
697 and therefore the fluorescent signal observed, ranging from 15- to 21-days, depending on the
698 molecule being expressed, likely corresponds to the persistence of the protein synthesized
699 during the time window of mRNA expression. The persistence of the reporter proteins is in
700 line with the fact that proteins involved in spermatogenesis exhibit a markedly low turnover
701 rate [31]. This is due to the fact that these proteins are stored within sperm organelles, such
702 as the acrosome, manchette, centrioles or fibrous sheath. These organelles, made during
703 spermiogenesis, remain stable for weeks until the fertilization process occurs because there
704 is no protein synthesis in mature sperm. For example, the $Ca_v3.2$ calcium channel is expressed
705 during meiosis at the pachytene stage and contributes to calcium signaling during acrosome
706 reaction [32-35]. When using the EEV vector, expression persisted for longer – up to 119 days
707 – due to the intrinsic property of the EEV plasmid which allows its replication in synchronous
708 manner with the host genome.

709 These results suggest that although EEV expression lasted longer, mRNAs, by targeting more
710 efficiently male germ cells and allowing higher transfection yields of seminiferous tubules,
711 could be a more effective and potent tool to express exogenous proteins in germ cells. By
712 expressing a missing protein in the case of male infertility due to monogenic causes, it could
713 be possible to restore failed spermatogenesis and thus to treat infertility.

714 **ARMC2 is expressed in late spermatogenesis stages**

715 We show that ARMC2 was localized in the flagellum of spermatids obtained by enzymatic
716 dissociation. No *Armc2* expression was detected in earlier germ cell type lineages like
717 spermatogonia or spermatocytes. These results suggest that the ARMC2 protein is expressed
718 late during spermatogenesis, which explains why motile sperm were found in the cauda
719 epididymis from 3-weeks after injection in our treated mice. Indeed, full spermiogenesis (from

720 round cells to sperm) takes around 15 days [36], and the journey across the epididymis lasts
721 around 8 days, making a total of 3-weeks. Our results also confirm those recently published
722 by Lechtreck et al. [37] from their study of the role of ARMC2 in the Intra-Flagellar Transport
723 (IFT) of radial spokes in *Chlamydomonas.* They suggested that the transport of the radial
724 spokes along the flagellum involves ARMC2, acting as an IFT adapter [37]. The presence of
725 ARMC2 in the flagella of elongating spermatid supports this hypothesis.
726
727 **Exogenous *Armc2*-mRNA expression rescued the motility of oligo-astheno-**
728 **teratozoospermic sperm**
729 This is the first demonstration that proteins can be expressed in the testis following
730 electroporation with optimized, capped and poly(A)-tailed mRNA.
731 Our objective was to develop a new targeted therapeutic approach for infertility associated
732 with monogenic defects. The objective of this preclinical study was to ascertain the efficacy of
733 messenger RNA (mRNA) in expressing a missing protein, ARMC2, in a mouse model exhibiting
734 oligo-astheno-teratozospermia due to the absence of *Armc2*, with the aim of restoring
735 flagellar motility and fertility. Our results strongly suggest that the strategy did not alter
736 spermatogenesis, as injection and electroporation of *Armc2*-mRNA or EEV-*Armc2* had no
737 effect on testicular morphology or weight. More importantly, the technique was effective,
738 with motile sperm cells found in cauda epididymis 3 and 5 weeks after *Armc2*-mRNA injection
739 into testes from *Armc2* KO males. Nevertheless, it should be noted that not all injected mice
740 were efficiently treated. For example, only 87.5% of the treated mice (14 of the 16) exhibited
741 motile sperm after 5 weeks. The absence of motile sperm at 5 weeks may be attributed to the
742 specific types of spermatogenic cells that were transfected during the electroporation phase.
743 It is possible that the transfected cells may differ between individuals, potentially influenced
744 by the injection and the position of the electrodes during electroporation. If the mRNA
745 transfection occurs in a spermatogonia, it may take more than six weeks (including the time
746 required to cross the epididymis) before motile epididymal sperm cells emerge. This potential
747 timeline could explain the absence of motile sperm in some mice at 5 weeks.

748 Due to the quantity of motile sperm obtained, it was not possible to produce offspring through
749 natural mating. However, the *Armc2*$^{-/-}$-rescued sperm exhibited normal morphology, motility,
750 and *in vitro* fertility. Indeed, the *Armc2*$^{-/-}$-rescued motile spermatozoa have successfully

751 fertilized eggs and produced embryos that were capable of developing properly into
752 blastocysts. These results provide compelling evidence that the method can effectively
753 produce fertile sperm. It worth to note that the significant modifications of the CASA
754 parameters observed for rescued sperm did not impact their fertilizing potential. Naked mRNA
755 injection/electroporation is therefore a promising method to treat infertility. In contrast, no
756 motile spermatozoa were found after injection/electroporation of EEV-*Armc2*, confirming our
757 previous results suggesting that this nucleic tool does not efficiently enter or transfect germ
758 cells.

759 Despite this success, the transfection rate deserves to be improved to obtain a larger number
760 of sperm cells to produced offspring through natural mating. To increase the testicular
761 transfection rate, encapsulation of mRNA into lipids nanoparticles could be used, as used for
762 Covid vaccination [38]. During the writing of this manuscript, Dong team [39], used a self-
763 amplifying RNA (saRNA) encapsulated in cholesterol-amino-phosphate derived lipid
764 nanoparticle to restore spermatogenesis in infertile mice. They successfully restore the
765 expression of the DNA Meiotic Recombinase 1 (DMC1) [40-42] in *Dmc1* KO infertile mice by
766 injecting a self-amplifying RNA-*Dmc1* in the testes. saRNA are genetically engineered replicons
767 derived from self-replicating single-stranded RNA viruses [43]. The saRNA contains the
768 alphavirus replicase genes and encodes an RNA-dependent RNA polymerase (RdRP) complex
769 which amplifies synthetic transcripts in situ and the target RNA sequence. The target RNA is
770 expressed at high levels as a separate entity. As a result of their self-replicative activity, saRNAs
771 can be delivered at lower concentrations than conventional mRNA to achieve comparable
772 expression levels [44]. Moreover, saRNA constructs need to be condensed by a cationic carrier
773 into a nanoparticle measuring ~100 nm to enable their uptake into target cells and protect the
774 saRNA from degradation [45]. Finally, saRNA will amplify the RNA without cellular regulation.
775 For all these reasons, if such a strategy is to be pursued, a potential toxicity effect due to
776 saRNA over expression must be investigated in the testes and progeny. Another difficulty with
777 saRNA relates to the size of the molecular construct. saRNA sequences are large and complex.
778 The length of the sequence RdRP is around 7 kilobases, which often makes the full length of
779 saRNA more than 9 kilobases once the sequence for the protein of interest has been
780 integrated [45]. Dong et al. [39] successfully used their saRNA construct to rescue
781 spermatogenesis failure induced by the absence of the small protein Dmc1 (37 KDa), but it

782 may be more challenging with larger proteins such as the structural proteins involved in OAT,
783 including the 98-kDa ARMC2 [23].
784 Our next step will be to assess whether encapsulating *Armc2*-mRNA in LNP-CAP could allow a
785 larger number of germ cells to be transfected.

786 **Naked mRNA, a new therapeutic strategy to treat severe infertility**

787 Non-obstructive Azoospermia (NOA) and severe oligozoospermia (SO) are the most severe
788 disorders of spermatogenesis and are the most likely to be of genetic origin. NOA is defined
789 by the complete absence of spermatozoa in the ejaculate. Approximately 10–15 % of infertile
790 men have azoospermia, and a further 15 % have SO [46]. For patients with NOA, few clinical
791 solutions are currently available. Generally, testicular sperm extraction is attempted to collect
792 some spermatozoa from the seminiferous tubules, which can then be used for ICSI [47]. When
793 no sperm are retrieved, intra-conjugal conception is impossible. The results of this study
794 strongly suggest that transient mRNA expression of a missing protein in NOA testes by
795 electroporation could be sufficient to produce normal sperm for IVF and obtain embryos.

796 In conclusion, this paper presents the first *in vivo* testicular injection and electroporation of
797 capped and poly(A)-tailed mRNA, demonstrating that it is an efficient strategy to transfect
798 male germ cells and that the duration of the expression of the resulting proteins is compatible
799 with restoring spermatogenesis. Our comprehensive study revealed mRNA to be more
800 efficient than an episomal vector, despite longer-lived expression in male germ cells with EEV.
801 The difference was linked to EEV achieving a lower rate of seminiferous tubule transfection
802 and a shorter duration of expression in germ cells. Our findings have also demonstrated, for
803 the first time, that sperm motility and fertility can be restored in mice with an oligo-astheno-
804 teratozoospermia phenotype through a technique that combines injection and
805 electroporation of capped and poly(A)-tailed mRNA. The findings presented open new
806 opportunities to develop efficient strategies to treat male infertility with monogenic causes.

807

808

809 **Legends**

810 **Figure 1: Distribution of I-particles NIRFIP-180 in testis injected *via* the rete testis route.**

811 (A) A solution containing 0.05 % Fast Green and 1 % fluorescent i-particles NIRFiP-180 was
812 prepared, 10 µL was injected into the seminiferous tubules of adult males, through the *rete*
813 *testes* and its efferent channels. Injection was performed at constant pressure under a
814 binocular microscope. The progression of filling of the seminiferous tubules was monitored
815 thanks to the Fast Green. (B) The testes were only filled to 2/3 capacity in order to prevent
816 damage to the tissue. (C) Representative distribution of fluorescent i-particles NIRFiP-180 in a
817 whole cross-section of an injected testis. Nuclei were counterstained with DAPI (blue
818 emission) to reveal tubules. (D) Enlargement of a seminiferous tubule showing particles
819 localized inside the lumens of the tubules. Scales bars: 1 mm and 500 µm.

820 **Figure 2: *In vivo* injection and electroporation do not alter the morphological structure of**
821 **the testes, seminiferous tubules, or sperm cells.**

822 (A, B) Testicular morphology was not affected by *in vivo* injection and electroporation of EEV-
823 *GFP* (A) or *GFP*-mRNA (B). Controls correspond to contralateral testes injected/electroporated
824 with control solution (PBS, 0.05 % FG). (A1, B1) comparison of the testicular morphology of
825 adult testes injected with nucleic acid vectors or control solutions. (A2, B2) Comparison of
826 testicular weight and (A3, B3) testicular length on day 7 after injection/electroporation. Data
827 are represented as a box plot median (n=4 for each condition). A Wilcoxon matched pairs test
828 was used to assess the significance of any differences in testis weights and lengths, and p
829 values of ≤ 0.05 were considered statistically significant. (C) Intact testicular structure after *in*
830 *vivo* injection and electroporation with EEV-*GFP* and *GFP*-mRNA. Comparison of testicular
831 cross section structures. Testes paraffin sections were stained with eosin/hematoxylin and
832 observed by light microscopy (20x magnification). (C1) Control, (C2) EEV-*GFP* injected and (C3)
833 *GFP*-mRNA injected. Scales bars: 1000 µm.

834 (D) Seminiferous tubule structures are not affected by *in vivo* injection and electroporation
835 with EEV-*GFP* and *GFP*-mRNA. Enlargement of cross sections showing the fine structure of a
836 seminiferous tubule for control (D1), EEV-*GFP* (D2) and *GFP*-mRNA (D3). In each tubule the
837 different layers of spermatogenic cells are indicated, Sertoli cells (S), Spermatogonia (Sg),

838 Spermatocytes (Scytes), rounds Spermatids (Stids) and sperm cells (Spz), Leydig cells (L).
839 Scales bars: 20 µm.

840 (E) The area of seminiferous tubules is not affected by *in vivo* injection and electroporation
841 with EEV-*GFP* and *GFP*-mRNA. Comparison of the seminiferous tubule diameter after injection
842 of nucleic acid vectors or control solutions. Data are represented as a box plot median. The
843 areas of seminiferous tubules (μm^2) were measured for round cross sections of $n > 35$ tubules
844 per testis section (n= 5 testis sections per condition). Statistical significance was verified using
845 a Student's *t*-test.

846 (F) Injection/electroporation do not impact epidydimal sperm cells. Representative sperm
847 observed by light microscopy on day 7 after injection/electroporation with Control solution
848 (F1), EEV-*GFP* (F2), or *GFP*-mRNA (F3). Scale bars: 10 µm. (F4) Percentage of normal
849 epidydimal sperm cells in each condition. The number of males were n=5 for EEV-*GFP*; n=6 for
850 *GFP*-mRNA and n=9 for WT. More than 150 sperm by males were analyzed. Statistical
851 significance was verified using a one-way ANOVA test.

852 **Figure 3: Kinetics of EEV-*GFP* expression following *in vivo* injection/electroporation: whole**
853 **testicular expression**

854 (A1-H1) Whole-mount testes on days 0, 1, 7, 14, 21, 28, 35 and 42 after *in vivo*
855 injection/electroporation with EEV-*GFP*. (A2-H2) Under fluorescence observation, GFP
856 expression was detectable in transfected testes from 12-week-old B6D2 mice. (C3-H3) Insets
857 show the absence of autofluorescence in non-transfected control testes, observed under 4X
858 magnification. The GFP expression presented a punctiform pattern in seminiferous tubules
859 and was detected from 1 day to 42 days. Scales bars: 1 mm and 100 µm.

860 **Figure 4: Kinetics of *GFP*-mRNA expression following *in vivo* injection/electroporation:**
861 **whole testicular expression**

862 (A1-F1) Whole-mount testes on days 0, 1, 7, 15, 21 and 28 after *in vivo* injection/
863 electroporation with *GFP*-mRNA. (A2-F2) Under fluorescence observation, GFP expression was
864 detectable in transfected testes from 12-week-old B6D2 mice. (A3-F3) Insets show the
865 absence of autofluorescence in non-transfected control testes, observed under 4X
866 magnification. The GFP expression presented a continuous pattern in seminiferous tubules
867 and was detected from day 1 to day 15. Scale bars: 1 mm and 100 µm.

868 (G) Comparison of the percentage of injected mice exhibiting reporter gene expression. Mice
869 injected with *GFP*-mRNA exhibited GFP expression from day 1 to day 21. Mice injected with
870 EEV-GFP exhibited GFP expression from day 1 to day 49. (for EEV-*GFP* n=11 on day 1; n=13 on
871 day 2; n=10 on day 3; n=14 on day 7; n= 5 on day 10; n= 12 on day 15; n=11 on day 21; n= 12
872 on day 28; n=15 on day 35; n=17 on day 42 and n=9 on day 49) ; (for *GFP*-mRNA n=3 on day
873 1; n=4 on day 3; n=15 on day 7; n= 21 on day 15; n=15 on day 21 and n= 5 on day 28).

874 **Figure 5: Kinetics of EEV and mRNA expression by *in vivo* bioluminescence imaging.**

875 (A) *In vivo* bioluminescence imaging quantification of luciferase expression over time following
876 injection/electroporation of EEV-*GFP-luc*. (A1) EEV-*GFP-Luc* was injected into the testes and
877 electroporated on day 0. Bioluminescence signal was quantified at several time points. Results
878 are expressed as a percentage of the maximal signal (mean ± SEM; n=5 mice up to D2; n=4
879 from D3 to D28; n=3 from D35 to D98 and n=3 from D105 to D119). (A2) *In vivo*
880 bioluminescence images of a representative mouse at several time points after administering
881 EEV-*GFP-LUC* or PBS, and ex vivo bioluminescence images of testes after 119 days.

882 (B) *In vivo* bioluminescence imaging quantification of luciferase expression over time induced
883 by injection/electroporation of *LUC*-mRNA**.** (B1) *LUC*-mRNA was injected into the testes and
884 electroporated on day 0. Bioluminescence signal was quantified in the whole testis at several
885 time points. Results are expressed as a percentage of the maximal signal (mean ± SEM; n = 5
886 mice). (B2) *In vivo* bioluminescence images of a representative mouse at several time points
887 after administering *LUC*-mRNA or PBS, and *ex vivo* bioluminescence images of caput, testes,
888 and cauda after 28 days.

889 (C) Decay over time of the number of mice expressing reporter genes. Mice were injected on
890 day 0 with *LUC*-mRNA or EEV-*GFP-LUC* and the number of mice showing bioluminescence in
891 the testis was counted at different time points, from day 1 to day 119. For EEV-*GFP*: n=13 at
892 D1; n=13 at D2; n=4 from D3 to D28; n=3 from D35 to D98 and n=3 from D105 to D119. For
893 *LUC*-mRNA: n = 5 mice for all-time points.

894 **Figure 6: Testicular and cellular *GFP*-mRNA expression measured on optically cleared testis**
895 **after 3D image reconstructions from lightsheet microscopy imaging.** Testes were
896 injected/electroporated with *GFP*-mRNA on day 0. On day 1, whole testes were fixed and
897 subjected to optical clearing. (A) Testes were observed before and after optical clearing on a

898 binocular microscope. The right image shows the transparency of the testis after complete
899 clearing, revealing the blue mesh throughout the organ. (B) The 3D internal structure of a
900 cleared testis was reconstructed from the lightsheet microscopy images. The reconstruction
901 was possible only for a half testis due to optical issues. Two opposing faces of the same testis
902 are presented, allowing the distribution of GFP fluorescence throughout the seminiferous
903 tubules to be measured. Pink fluorescence corresponds to the autofluorescence of interstitial
904 cells located around the seminiferous tubules. Scale bars A: 1 mm and B: 500 µm.
905
906 **Figure 7: Cellular expression of EEV-*GFP* following *in vivo* injection/ electroporation**. Testes
907 were injected/electroporated with EEV-*GFP* on day 0. On day 1 and on day 7, whole testes
908 were fixed and subjected to optical clearing. Cleared tested were observed by fluorescence
909 microscopy. (A1-A3) On day 1, transfected seminiferous tubules showed dotted green
910 fluorescence at low magnification (10x/0.45). Nuclei were counterstained with DAPI (blue
911 staining) to reveal the structure of the seminiferous tubules. At the cellular level, fluorescence
912 was detectable (B1-B3) in germ cells including Spermatogonia (Sg), Spermatocytes (Scytes)
913 and round Spermatids (RStids), as well as (C1-C3) in Sertoli cells (SC). (D1-D3) On day 7, the
914 GFP signal was lower at low magnification (10x/0.45) and detectable (E1-E3) only in Sertoli
915 cells (40x/1.15 WI) (n=3) (PTc =Peri-tubular myoid cell). E4 is an enlargement of the red square
916 in E3, allowing the cell type to be identified. Scale bars: 100 µm, 15 µm and 3 µm.

917 **Figure 8: Cellular expression of *GFP*-mRNA following *in vivo* injection/electroporation**.
918 Testes were injected/electroporated with *GFP*-mRNA on day 0. On day 1 and day 7, whole
919 testes were fixed and subjected to optical clearing. Cleared testes were observed by
920 fluorescence microscopy. (A1-A3) On day 1, transfected seminiferous tubules showed strong
921 broad-ranging green fluorescence at low magnification (10x0/0.45). Nuclei were
922 counterstained with DAPI (blue staining) to reveal the structure of the seminiferous tubule. At
923 the cellular level, fluorescence was detectable in germ cells (B1-B3) including Spermatogonia
924 (Sg), Spermatocytes (Scytes) and round Spermatids (RStids), mature spermatids cells (m-
925 Sptids) and Sertoli cells (SC). B4 is an enlargement of the red square in B3, allowing the cell
926 types to be identified. (D1-D3) On day 7, the GFP signal remained strong at low magnification
927 (10x/0.45) and was still detectable in (E1-E3) all germ cell types and Sertoli cells (40x/1.15 WI)

928 (n=3). E4 is an enlargement of the red square in E3, showing that testicular sperm were also
929 stained. Scale bars: 100 µm, 15 µm and 3 µm.

930 **Figure 9: ARMC2 localization in dissociated testicular cells observed by**
931 **immunofluorescence.** Cells from WT and *Armc2* KO mice were counterstained with Hoechst
932 (A1-B1) and stained with antibodies against tubulin (A2-B2, green signal) and ARMC2 (A3-B3,
933 red signal). (A4-B4) overlay of the different staining. In WT mice, ARMC2 is located in the
934 flagellum of spermatids. In KO mice, no ARMC2 signal (red fluorescence) was observed in any
935 cells.

936 **Figure 10: *In vivo* co-injection of *Armc2*-mRNA and *eGFP*-mRNA followed by electroporation**
937 **do not affect testes morphology and weight.** Adult WT mouse testes were injected with a
938 solution containing *Armc2*-mRNA and *eGFP*-mRNA. After injection, the testes were
939 electroporated and mice were euthanized two weeks later. (A): Whole testis under white and
940 blue lights on a fluorescence microscope (A1): control testes not injected/electroporated (A2):
941 testes injected with *Armc2*-mRNA and *eGFP*-mRNA. *eGFP*-mRNA was co-injected to follow the
942 transfection efficiency. (B): Ratio of injected/electroporated testis weights to control testis
943 weights at several time points post-injection (3-, 6-, 10-, 15-, 21-, 28- and 35-days post-
944 surgery). n= 1 mouse per time.

945 **Figure 11: Sperm motility is restored in *Armc2* KO mice at 21 and 35 days after injection and**
946 **electroporation of *Armc2*-mRNA**. (A) Adult *Armc2* KO mouse testes were injected with a
947 solution containing *Armc2*-mRNA. After injection, the testes were electroporated. At different
948 times (3-, 6-, 10-, 15-, 21-, 28-, and 35-days *post*-injection), sperm were extracted from the
949 cauda epididymis of the injected testis, and the sample was then examined with a CASA
950 system to identify the percentage of motile spermatozoa (A1). n= 2 for day 15, n= 3 for days
951 3, 6 and 21, n= 4 for day 10, and n= 5 for days 28 and 35. (A2) Sperm motility parameters of
952 *Armc2*$^{-/-}$ -rescued sperm in comparison to *Armc2*$^{+/+}$ sperm. The motility parameters measured
953 were: averaged path velocity (VAP); straight line velocity (VSL); curvilinear velocity (VCL);
954 amplitude of lateral head displacement (ALH); beat cross frequency (BCF); straightness (STR);
955 linearity (LIN). Black dots: sperm cells from *Armc2* null mice, green dots: sperm cells from
956 *Armc2* null mice 35 days after injection with *Armc2*-mRNA. Results are expressed as
957 mean ± SD. (A3) Sperm motility population of *Armc2*$^{-/-}$ -rescued sperm in comparison to
958 *Armc2*$^{-/-}$ sperm. Black column: sperm cells from *Armc2* null mice, green column: sperm cells

959 from *Armc2* null mice 35 days after injection with *ARmc2*-mRNA. Statistical significance was
960 verified using a Mann-Whitney sum test. Data are displayed as mean ± SEM. P values of * ≤
961 0.05, ** ≤ 0.01, or *** ≤ 0.001 were considered to represent statistically significant
962 differences.

963 (B) Morphology of sperm cells in *Armc2* KO mice injected or not with *Armc2*-mRNA. (B1-B2):
964 microscopic observation of epididymal sperm cells from a mature WT mouse. (B3-B4):
965 epididymal sperm cells from a mature *Armc2* KO mouse 35 days after
966 injection/electroporation with *Armc2*-mRNA. (B5-B6): epididymal sperm cells from a control
967 *Armc2* KO male. Normal sperm cells were observed in the injected condition with *Armc2*-
968 mRNA. (White arrows), Scale bars: 10 µm.

969 **Fig 12: *Armc2* $^{-/-}$-rescued sperm can fertilize eggs and produce embryos by IVF and ICSI.**

970 (A) Armc2 $^{-/-}$-rescued sperm can fertilize eggs by IVF. (A1) Illustration of 2-cell embryo obtained
971 W/O sperm, by IVF with *Armc2*$^{-/-}$ sperm and by IVF with *Armc2*$^{-/-}$ rescued sperm; green
972 asterisks show 2-cell embryos obtained by fertilization, red asterisks show 2-cell embryos
973 obtained by parthenogenesis and white asterisks show unfertilized oocytes or degenerated.
974 (A2) Histograms showing the mean percentage ± SD of alive eggs reaching the 2-cell embryo
975 stage at 24 hours after IVF without sperm (n=4), with *Armc2*$^{-/-}$ sperm (n=4), and with *Armc2*$^{-/-}$
976 rescued sperm (n=5). Statistical significance was verified using a one-way ANOVA test. (B)
977 Comparative analysis of the percentage of blastocysts produced by ICSI with spermatozoa
978 from wild-type (WT), *Armc2*$^{-/-}$ and *Armc2*$^{-/-}$-rescued individuals. For *Armc2*$^{-/-}$-rescued
979 individuals, only motile sperm were injected. IVF and ICSI schemes were retrieved from
980 Biorender.

981 **Supp Fig 1: EEV and mRNA maps**

982 (A) EEV-plasmid map. The EEV-plasmid contains GFP, EVB ori, GFP, Luciferase, and EBNA
983 sequences under the control of the GAGs promotor. (B) The mCherry plasmid contains the
984 mCherry gene under the control of a T7 promotor. (C) The EEV-*Armc2* plasmid contains GFP,
985 oriP, EBNA and *Armc2* sequences under the control of the CMV and T7 promotors. (D)
986 *mCherry*-mRNA was synthesized as described in Material and Methods. It was validated by
987 agarose gel electrophoresis: Lane 1: DNA size marker ladder (100 bp), lane 2: capped *mCherry*-

988 mRNA (IVT product), lane 3: *mCherry*-mRNA after DNAse treatment. Capped and poly A tailed
989 *mCherry*-mRNA migrated to the expected size of 876 bp.

990 **Supp Fig 2: Damaged tubules observed by optical microscopy following overstimulation**

991 Adult mouse testes were *in vivo* injected and over electroporated using 10 square electric
992 pulses to induce damage. (A) Control testis (no injection/electroporation). (B1-B2) Over
993 electroporated testes showing damaged tubules as pearly white striations. Scale bars: 1 mm.

994 **Supp Fig 3: Testicular expression of *mCherry*-mRNA following in vivo electroporation**

995 (A1, B1, C1, D1, E1 and F1) Whole-mount testes on days 0, 1, 7, 14, 21, 28 after *in vivo*
996 injection/ electroporation. (A2, B2, C2, D2, E2 and, F2) Using fluorescence microscopy,
997 transfected testes from 12-week-old B6D2 mice express red mCherry fluorescence. mCherry
998 was detected in a diffuse pattern throughout the seminiferous tubules from day 1 to day 15.
999 (A3, B3, C3, D3, E3 and F3) images showing the absence of autofluorescence in non-
1000 transfected control testes observed at 4x magnification. Scales bars: 1 mm and 100 µm.

1001 **Supp Fig 4: Cellular expression of *mCherry*-mRNA following in vivo injection/**
1002 **electroporation.**
1003 Cross sections (20 µm) of mouse testes on day 1 (AB) and day 7 (CD) after in vivo injection and
1004 electroporation with *mCherry*-mRNA, observed under fluorescence microscopy. Red signals
1005 correspond to successfully transfected testicular tubular cells; nuclei were counterstained
1006 with DAPI (blue). At the cellular level, mCherry fluorescence was detectable in Sertoli cells
1007 (SC); Spermatogonia (SG); Spermatocytes (Scytes); round Spermatids (RStids), and mature
1008 spermatids (m-Sptids); Scale bars: 10 µm and 5 µm.
1009 **Supp Fig 5: Decay over time of the number of mice exhibiting reporter gene expression**
1010 **following injection/electroporation of the three different mRNAs.**

1011 Mice were injected on day 0 with *LUC*-mRNA, *GFP*-mRNA or *mCherry*-mRNA and the number
1012 of mice showing bioluminescence or fluorescence in the testis was counted at different time
1013 points. For *LUC*-mRNA n= 5 mice at each time point. For *mCherry*-mRNA n=3 on day 1; n=4 on
1014 day3; n=15 on day 7; n= 21 on day 15; n=15 on day 21; n= 5 on day 28; n=5 on day 35; and for
1015 *GFP*-mRNA n=3 on day 12; n=7 on day 2; n=7 on day 3; n=12 on day 7; n= 13 on day 15; n=10
1016 on day 21 ; n= 9 on day 28; n=17 on day 35 and n=5 on day 42.

1017 **Supp Fig 6: *Armc2* expression and localization in mice testis**

1018 (A) IF experiment on dissociated spermatogenic cell from WT male. (A1) Nuclei were
1019 counterstained with DAPI (blue staining), (A2) tubulin (green signal) and (A3) ARMC2 (red
1020 signal). (A4) overlay. ARMC2 is located in the flagellum of spermatids Scale bars: 5 µm. (B)
1021 Cross-sections of seminiferous tubules (B1) Nuclei were counterstained with DAPI (blue
1022 staining), (B2) and (B2) ARMC2 (red signal). (B3) overlay. B4 is an enlargement of the red
1023 square in B3, showing that only elongating/mature spermatids were stained. (C) Expression of
1024 *Armc2* in mouse spermatogenic cells based on the RNA-sequencing study from Gan et al. 2013.
1025 Primitive type A spermatogonia (priSG-A) were isolated from 6 dpp mice; Type A
1026 spermatogonia (SG-A) and type B spermatogonia (SG-B) were from 8 dpp mice; preleptotene
1027 spermatocytes (plpSC) and pachytene spermatocytes (pacSC) were from 17 dpp mice; and
1028 round spermatids (rST), elongating spermatids (eST) and spermatozoa (SZ) were from 60 dpp
1029 mice. Artificial units (AU). Dpp: day post-partum

1030 **Supp Fig 7: Validation of *Armc2*-mRNA in HEK cells.**

1031 HEK cells were transfected with *Armc2*-mRNA or EEV-*Armc2.* ARMC2 protein was detected by
1032 Western blot with an anti-HA primary antibody. The expected size of the ARMC2 protein is
1033 98 kDa**.**

1034 **Supp Fig 8: Morphology of sperm cells from WT, *Armc2* KO and *Armc2*-rescued males.**

1035 Microscopic observation of epididymal sperm cells from WT, *Armc2* KO and *Armc2* KO-*Armc2*-
1036 mRNA injected males at 20x (left column), 40x (middle column) and 100x (right column)
1037 magnifications. In the rescue condition, rescued sperm cells were labeled with a white
1038 asterisk. Scale bars: 100, 50 and 10 µm.

1039 **Videos 1 and 2: 3D-microscopic reconstructions of faces 1 and 2 of a testis injected with *GFP*-**
1040 **mRNA.**

1041 **Video 3: CASA recording of WT epidydimal sperm cells**

1042 **Video 4: CASA recording of *Armc2* KO epidydimal sperm cells**

1043 **Videos 5 and 6: CASA recordings of epidydimal sperm cells from *Armc2* KO mice on day 21**
1044 **and day 35, respectively, after injection/electroporation with *Armc2*-mRNA.**

Acknowledgments

This work was supported by CNRS, INSERM and ANR-20-CE18-0007 grant to JE. This work was supported by the Fondation pour la Recherche Médicale, grant number « ECO202006011669 » to CV.

We acknowledge the MicroCell facility (GIS IBiSA, ISdV, IAB), member of the national infrastructure France-BioImaging supported by the French National Research Agency (ANR-10-INBS-04)) for optical microscopy.

Bibliography

1. Boivin, J., et al., *International estimates of infertility prevalence and treatment-seeking: potential need and demand for infertility medical care.* Hum Reprod, 2007. **22**(6): p. 1506-12.
2. Thonneau, P. and A. Spira, *Prevalence of infertility: international data and problems of measurement.* Eur J Obstet Gynecol Reprod Biol, 1991. **38**(1): p. 43-52.
3. Kekalainen, J., *Genetic incompatibility of the reproductive partners: an evolutionary perspective on infertility.* Hum Reprod, 2021. **36**(12): p. 3028-3035.
4. Kumar, N. and A.K. Singh, *Trends of male factor infertility, an important cause of infertility: A review of literature.* J Hum Reprod Sci, 2015. **8**(4): p. 191-6.
5. Uhlen, M., et al., *Transcriptomics resources of human tissues and organs.* Mol Syst Biol, 2016. **12**(4): p. 862.
6. Thonneau, P., et al., *Incidence and main causes of infertility in a resident population (1,850,000) of three French regions (1988-1989).* Hum Reprod, 1991. **6**(6): p. 811-6.
7. Cavallini, G., *Male idiopathic oligoasthenoteratozoospermia.* Asian J Androl, 2006. **8**(2): p. 143-57.
8. Colpi, G.M., et al., *European Academy of Andrology guideline Management of oligo-astheno-teratozoospermia.* Andrology, 2018. **6**(4): p. 513-524.
9. Hansen, M., et al., *Assisted reproductive technologies and the risk of birth defects--a systematic review.* Hum Reprod, 2005. **20**(2): p. 328-38.
10. Halliday, J.L., et al., *Increased risk of blastogenesis birth defects, arising in the first 4 weeks of pregnancy, after assisted reproductive technologies.* Hum Reprod, 2010. **25**(1): p. 59-65.
11. Davies, M.J., et al., *Reproductive technologies and the risk of birth defects.* N Engl J Med, 2012. **366**(19): p. 1803-13.
12. Kurinczuk, J.J., M. Hansen, and C. Bower, *The risk of birth defects in children born after assisted reproductive technologies.* Curr Opin Obstet Gynecol, 2004. **16**(3): p. 201-9.
13. Usmani, A., et al., *A non-surgical approach for male germ cell mediated gene transmission through transgenesis.* Sci Rep, 2013. **3**: p. 3430.
14. Raina, A., et al., *Testis mediated gene transfer: in vitro transfection in goat testis by electroporation.* Gene, 2015. **554**(1): p. 96-100.
15. Michaelis, M., A. Sobczak, and J.M. Weitzel, *In vivo microinjection and electroporation of mouse testis.* J Vis Exp, 2014(90).
16. Wang, L., et al., *Testis electroporation coupled with autophagy inhibitor to treat non-obstructive azoospermia.* Mol Ther Nucleic Acids, 2022. **30**: p. 451-464.

1087 17. Duan, D., *Full-length dystrophin gene therapy for Duchenne muscular dystrophy.* Mol Ther,
1088 2024. **32**(9): p. 2817-2818.
1089 18. Jacobson, S.G., et al., *Safety and improved efficacy signals following gene therapy in childhood*
1090 *blindness caused by GUCY2D mutations.* iScience, 2021. **24**(5): p. 102409.
1091 19. Liu, S., *Legal reflections on the case of genome-edited babies.* Glob Health Res Policy, 2020. **5**:
1092 p. 24.
1093 20. Sadelain, M., E.P. Papapetrou, and F.D. Bushman, *Safe harbours for the integration of new DNA*
1094 *in the human genome.* Nat Rev Cancer, 2011. **12**(1): p. 51-8.
1095 21. Ishii, T., *Germ line genome editing in clinics: the approaches, objectives and global society.* Brief
1096 Funct Genomics, 2017. **16**(1): p. 46-56.
1097 22. Parhiz, H., E.N. Atochina-Vasserman, and D. Weissman, *mRNA-based therapeutics: looking*
1098 *beyond COVID-19 vaccines.* Lancet, 2024. **403**(10432): p. 1192-1204.
1099 23. Coutton, C., et al., *Bi-allelic Mutations in ARMC2 Lead to Severe Astheno-Teratozoospermia*
1100 *Due to Sperm Flagellum Malformations in Humans and Mice.* Am J Hum Genet, 2019. **104**(2):
1101 p. 331-340.
1102 24. in *Transforming and Scaling Up Health Professionals' Education and Training: World Health*
1103 *Organization Guidelines 2013*. 2013: Geneva.
1104 25. Schindelin, J., et al., *Fiji: an open-source platform for biological-image analysis.* Nat Methods,
1105 2012. **9**(7): p. 676-82.
1106 26. Yoshida, N. and A.C. Perry, *Piezo-actuated mouse intracytoplasmic sperm injection (ICSI).*
1107 Nat.Protoc., 2007. **2**(2): p. 296-304.
1108 27. Ruthig, V.A. and D.J. Lamb, *Updates in Sertoli Cell-Mediated Signaling During Spermatogenesis*
1109 *and Advances in Restoring Sertoli Cell Function.* Front Endocrinol (Lausanne), 2022. **13**: p.
1110 897196.
1111 28. de Boer, P., M. de Vries, and L. Ramos, *A mutation study of sperm head shape and motility in*
1112 *the mouse: lessons for the clinic.* Andrology, 2015. **3**(2): p. 174-202.
1113 29. Gan, H., et al., *Dynamics of 5-hydroxymethylcytosine during mouse spermatogenesis.* Nat
1114 Commun, 2013. **4**: p. 1995.
1115 30. Liu, A. and X. Wang, *The Pivotal Role of Chemical Modifications in mRNA Therapeutics.* Front
1116 Cell Dev Biol, 2022. **10**: p. 901510.
1117 31. Hermann, B.P., et al., *The Mammalian Spermatogenesis Single-Cell Transcriptome, from*
1118 *Spermatogonial Stem Cells to Spermatids.* Cell Rep, 2018. **25**(6): p. 1650-1667 e8.
1119 32. Arnoult, C., et al., *Control of the low voltage-activated calcium channel of mouse sperm by egg*
1120 *ZP3 and by membrane hyperpolarization during capacitation.* Proc Natl Acad Sci U S A, 1999.
1121 **96**(12): p. 6757-62.
1122 33. Escoffier, J., et al., *Expression, localization and functions in acrosome reaction and sperm*
1123 *motility of Ca(V)3.1 and Ca(V)3.2 channels in sperm cells: an evaluation from Ca(V)3.1 and*
1124 *Ca(V)3.2 deficient mice.* J Cell Physiol, 2007. **212**(3): p. 753-63.
1125 34. Saunders, C.M., et al., *PLC zeta: a sperm-specific trigger of Ca(2+) oscillations in eggs and*
1126 *embryo development.* Development, 2002. **129**(15): p. 3533-44.
1127 35. Saunders, C.M., K. Swann, and F.A. Lai, *PLCzeta, a sperm-specific PLC and its potential role in*
1128 *fertilization.* Biochem Soc Symp, 2007(74): p. 23-36.
1129 36. Ibtisham, F., et al., *Progress and future prospect of in vitro spermatogenesis.* Oncotarget, 2017.
1130 **8**(39): p. 66709-66727.
1131 37. Lechtreck, K.F., et al., *Chlamydomonas ARMC2/PF27 is an obligate cargo adapter for*
1132 *intraflagellar transport of radial spokes.* Elife, 2022. **11**.
1133 38. Schoenmaker, L., et al., *mRNA-lipid nanoparticle COVID-19 vaccines: Structure and stability.* Int
1134 J Pharm, 2021. **601**: p. 120586.
1135 39. Du, S., et al., *Cholesterol-Amino-Phosphate (CAP) Derived Lipid Nanoparticles for Delivery of*
1136 *Self-Amplifying RNA and Restoration of Spermatogenesis in Infertile Mice.* Adv Sci (Weinh),
1137 2023. **10**(11): p. e2300188.

1138 40. Takemoto, K., et al., *Meiosis-Specific C19orf57/4930432K21Rik/BRME1 Modulates Localization*
1139 *of RAD51 and DMC1 to DSBs in Mouse Meiotic Recombination.* Cell Rep, 2020. **31**(8): p. 107686.
1140 41. Habu, T., et al., *The mouse and human homologs of DMC1, the yeast meiosis-specific*
1141 *homologous recombination gene, have a common unique form of exon-skipped transcript in*
1142 *meiosis.* Nucleic Acids Res, 1996. **24**(3): p. 470-7.
1143 42. Shinohara, A., et al., *Saccharomyces cerevisiae recA homologues RAD51 and DMC1 have both*
1144 *distinct and overlapping roles in meiotic recombination.* Genes Cells, 1997. **2**(10): p. 615-29.
1145 43. Tews, B.A. and G. Meyers, *Self-Replicating RNA.* Methods Mol Biol, 2017. **1499**: p. 15-35.
1146 44. Bloom, K., F. van den Berg, and P. Arbuthnot, *Self-amplifying RNA vaccines for infectious*
1147 *diseases.* Gene Ther, 2021. **28**(3-4): p. 117-129.
1148 45. Kim, J., et al., *Self-assembled mRNA vaccines.* Adv Drug Deliv Rev, 2021. **170**: p. 83-112.
1149 46. Cocuzza, M., C. Alvarenga, and R. Pagani, *The epidemiology and etiology of azoospermia.*
1150 Clinics (Sao Paulo), 2013. **68 Suppl 1**: p. 15-26.
1151 47. Ma, Y., et al., *A risk prediction model of sperm retrieval failure with fine needle aspiration in*
1152 *males with non-obstructive azoospermia.* Hum Reprod, 2019. **34**(2): p. 200-208.

1153

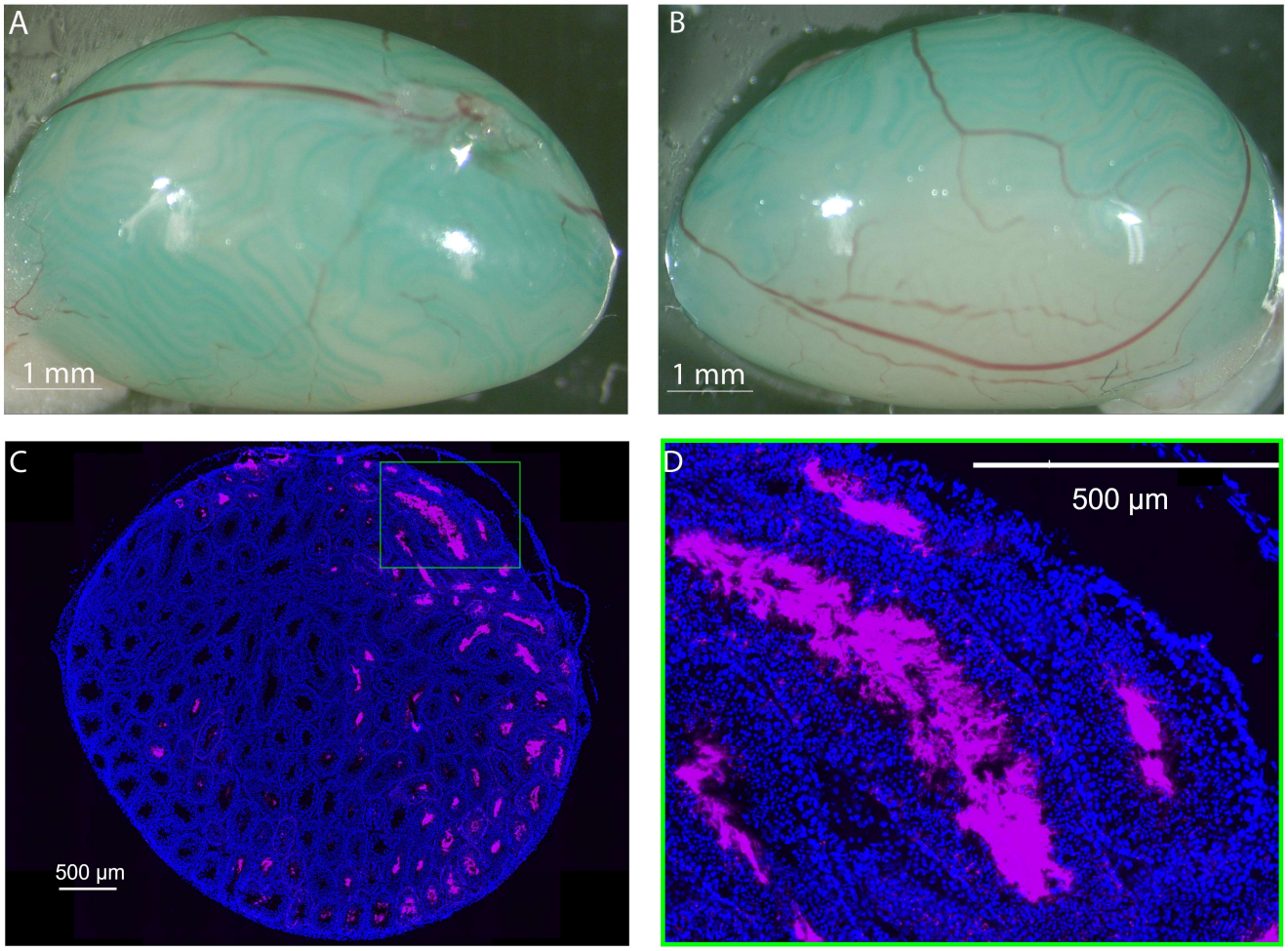

Figure 1, Vilpreux et al 2023

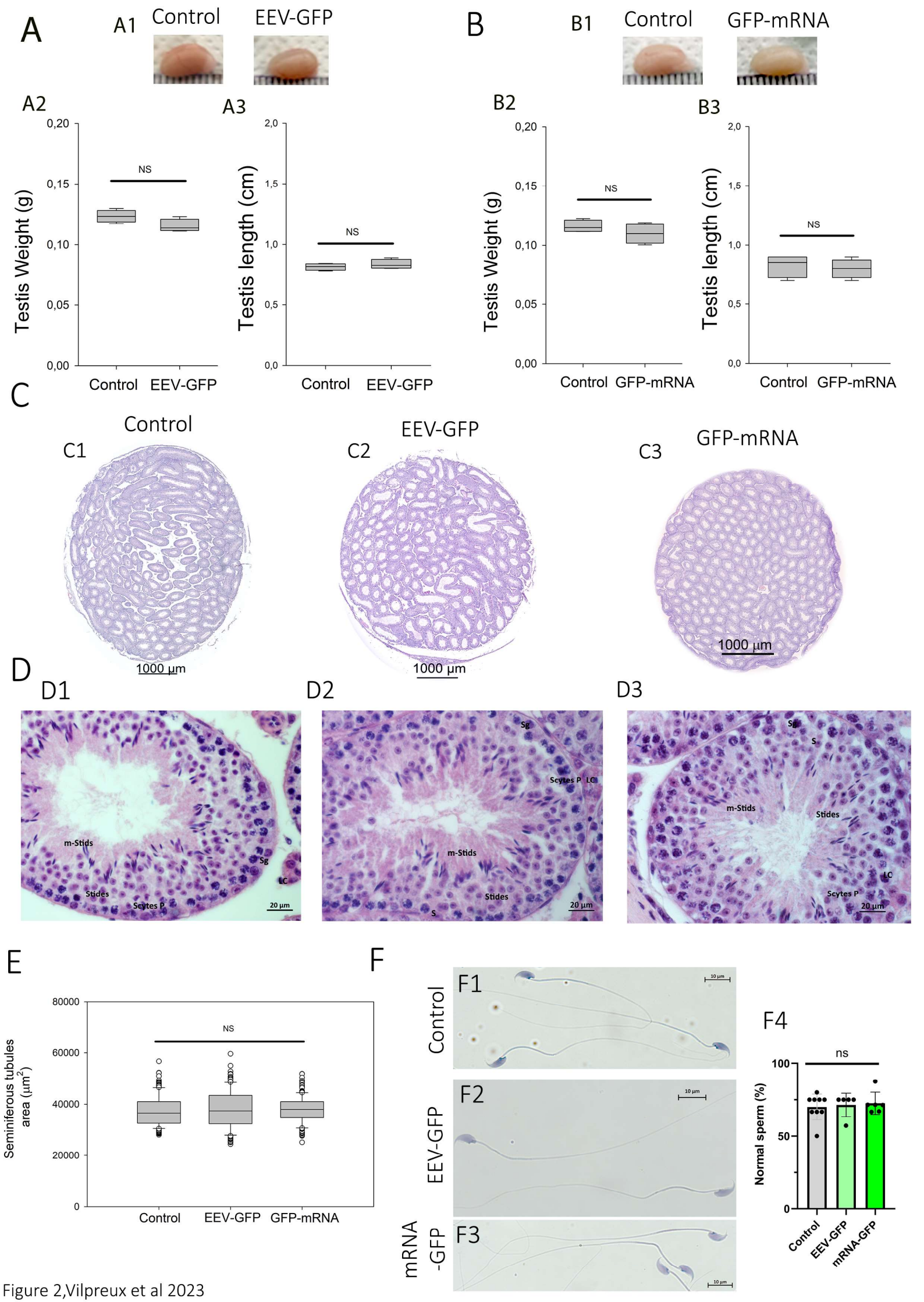

Figure 2,Vilpreux et al 2023

EEV-GFP

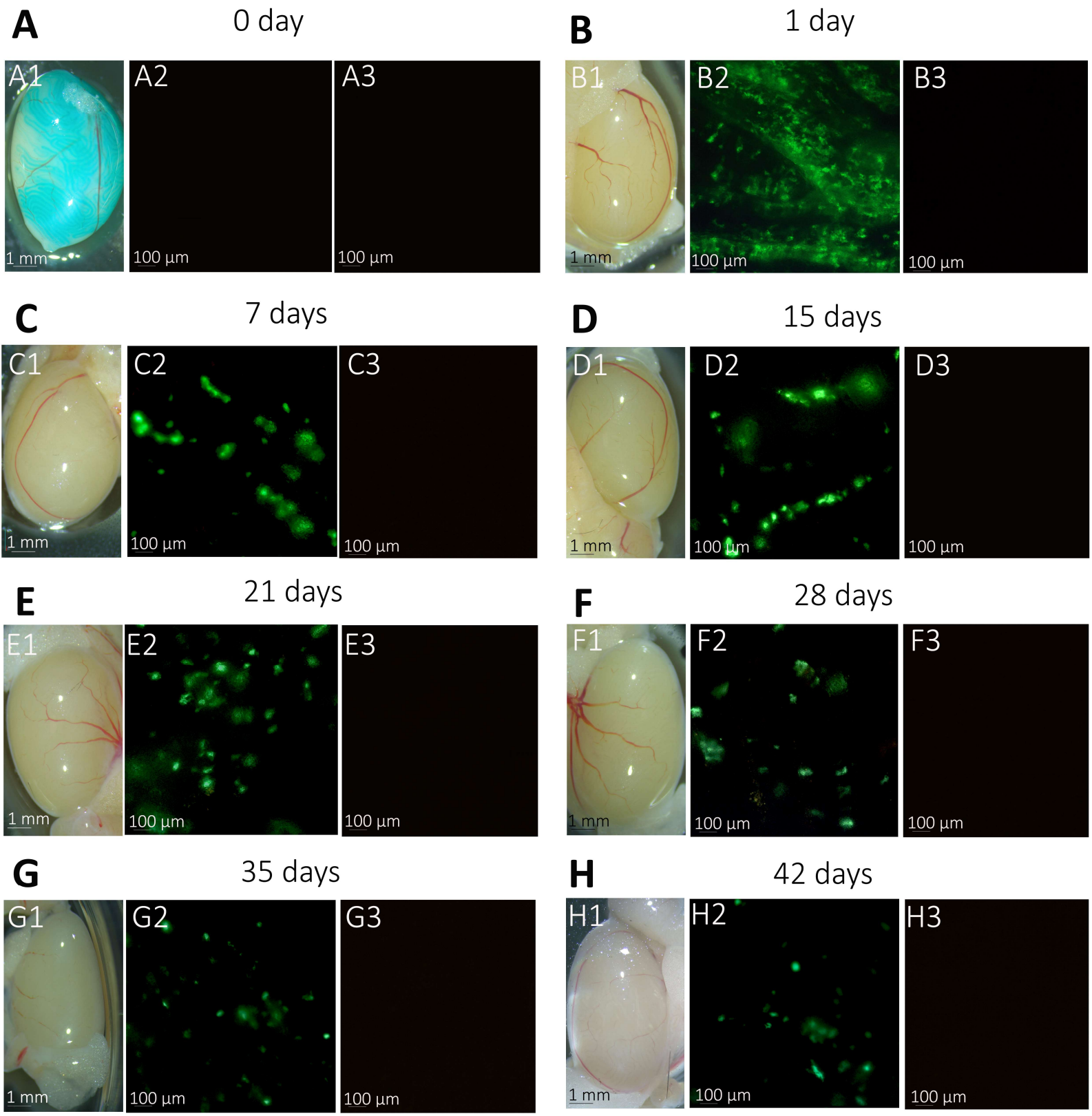

Figure 3,Vilpreux et al 2023

GFP-mRNA

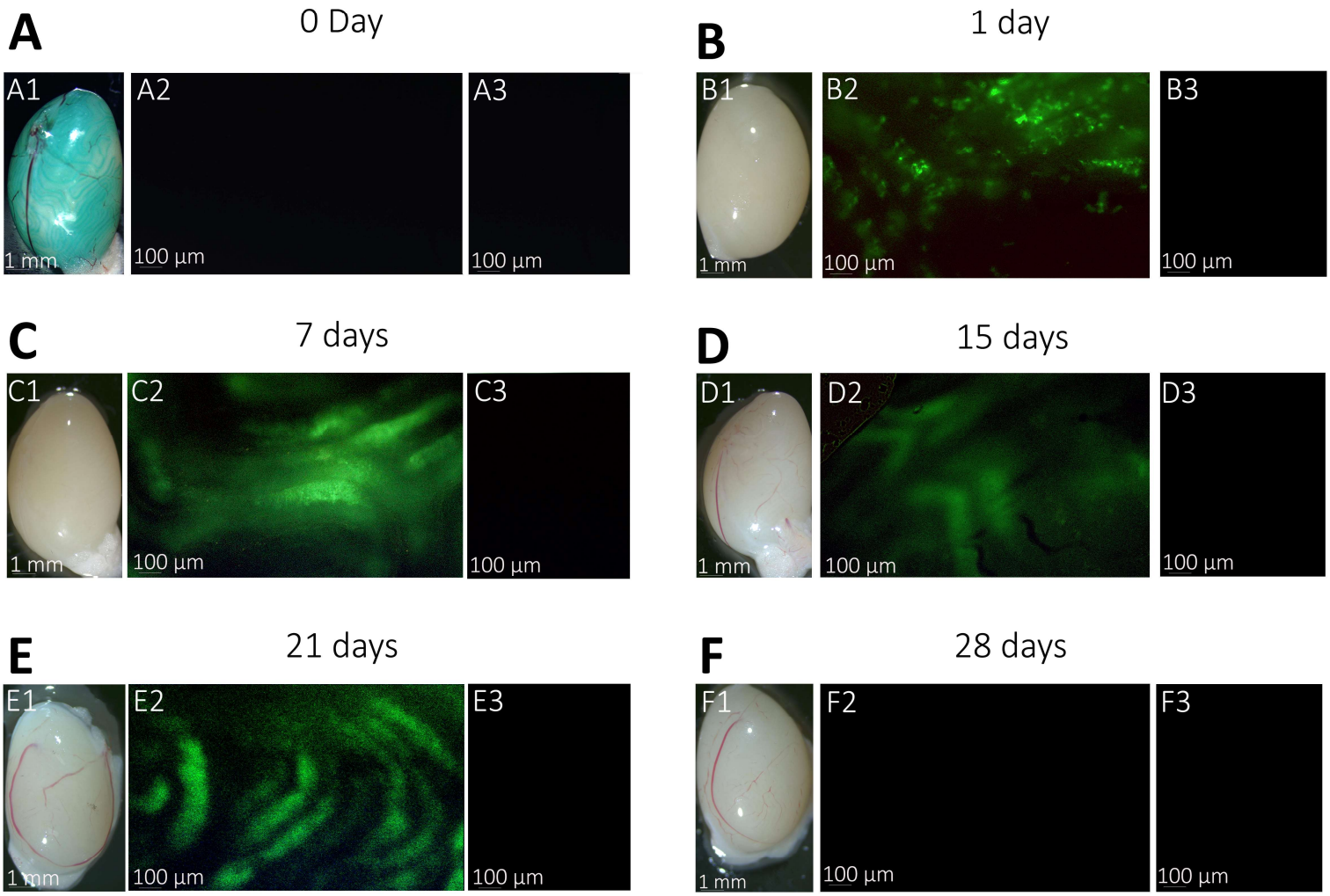

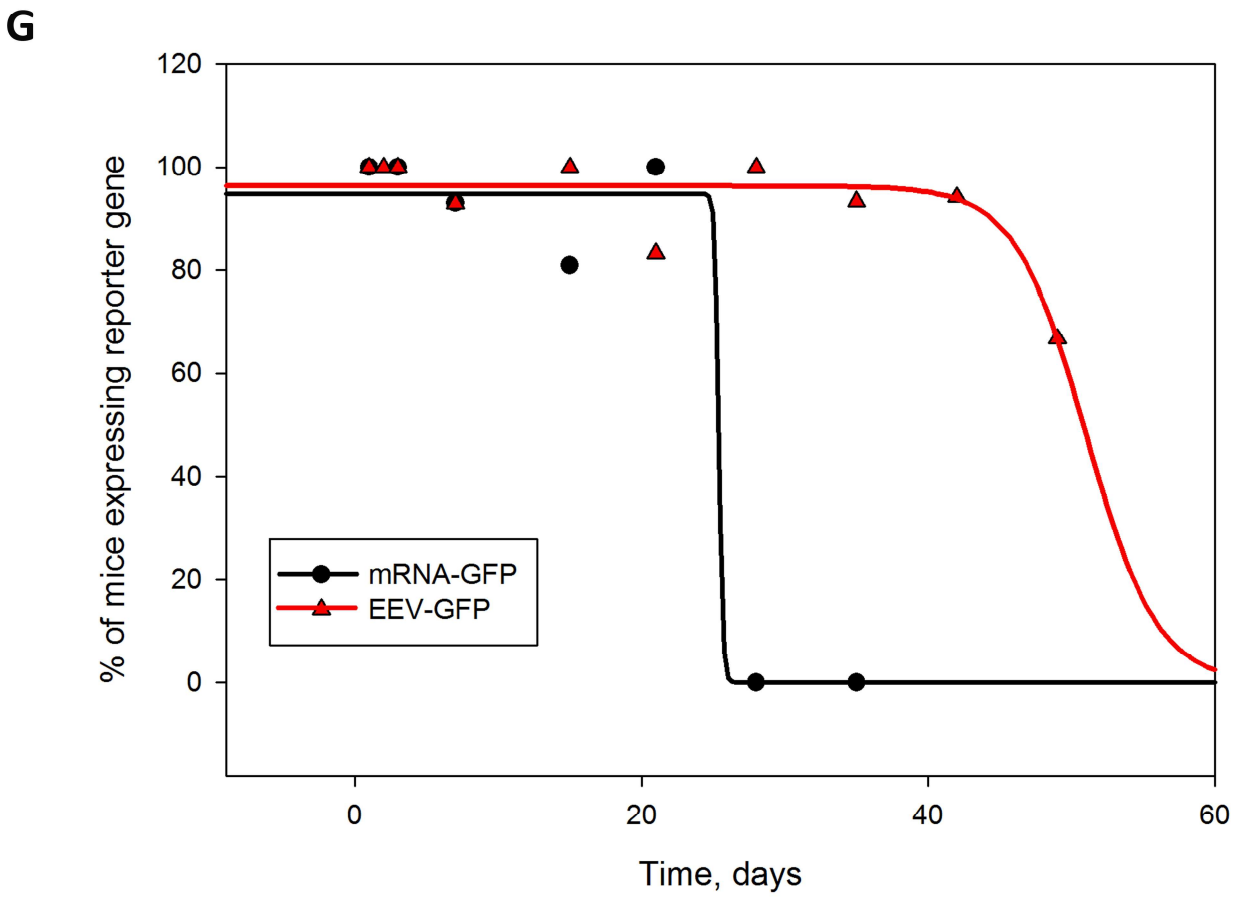

Fig4, Vilpreux et al 2023

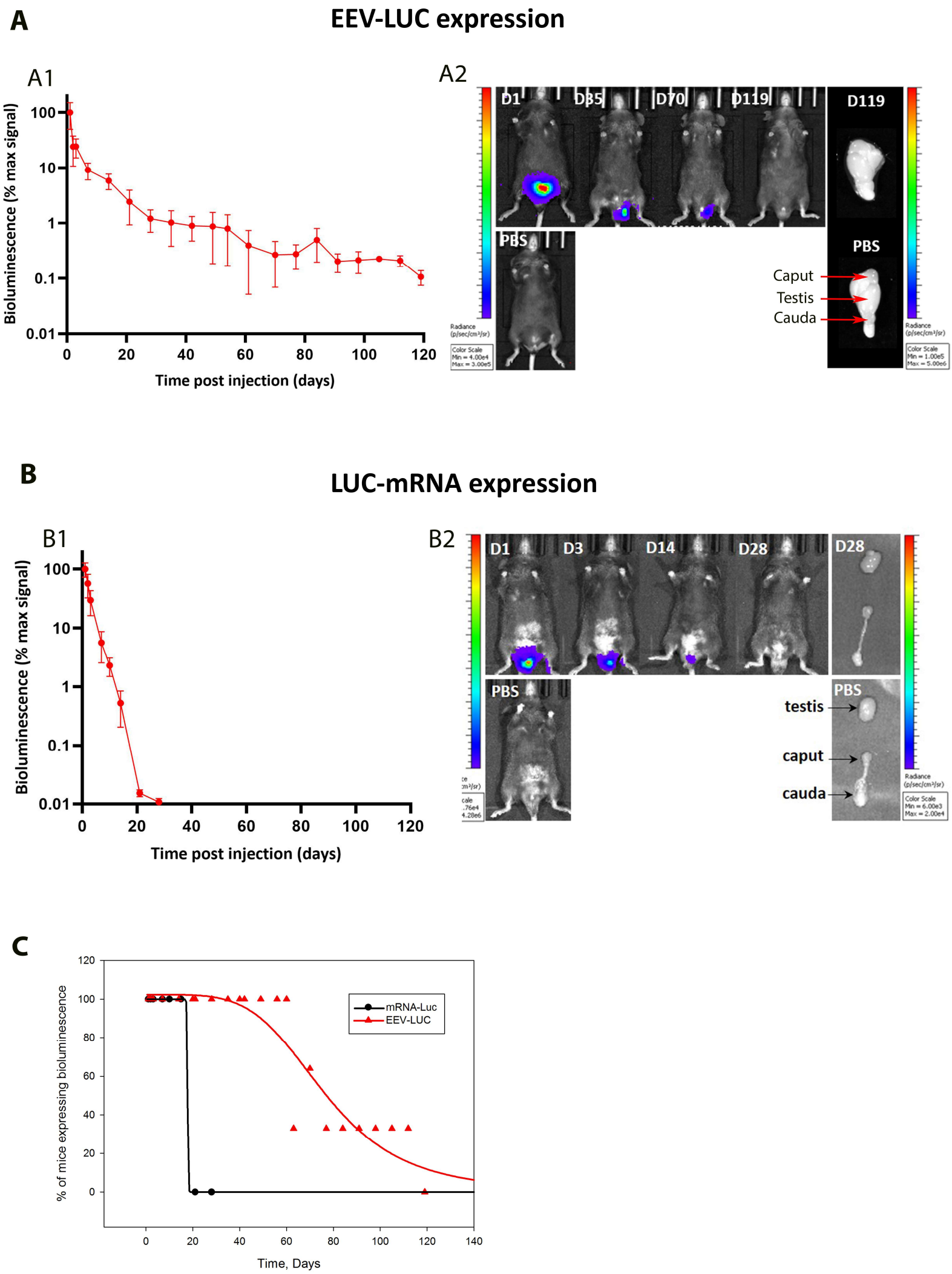

Figure 5, Vilpreux et al 2023

GFP-mRNA 1 day post injection

A

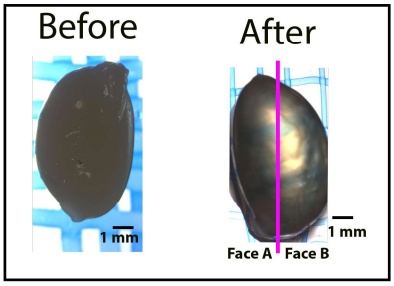

B

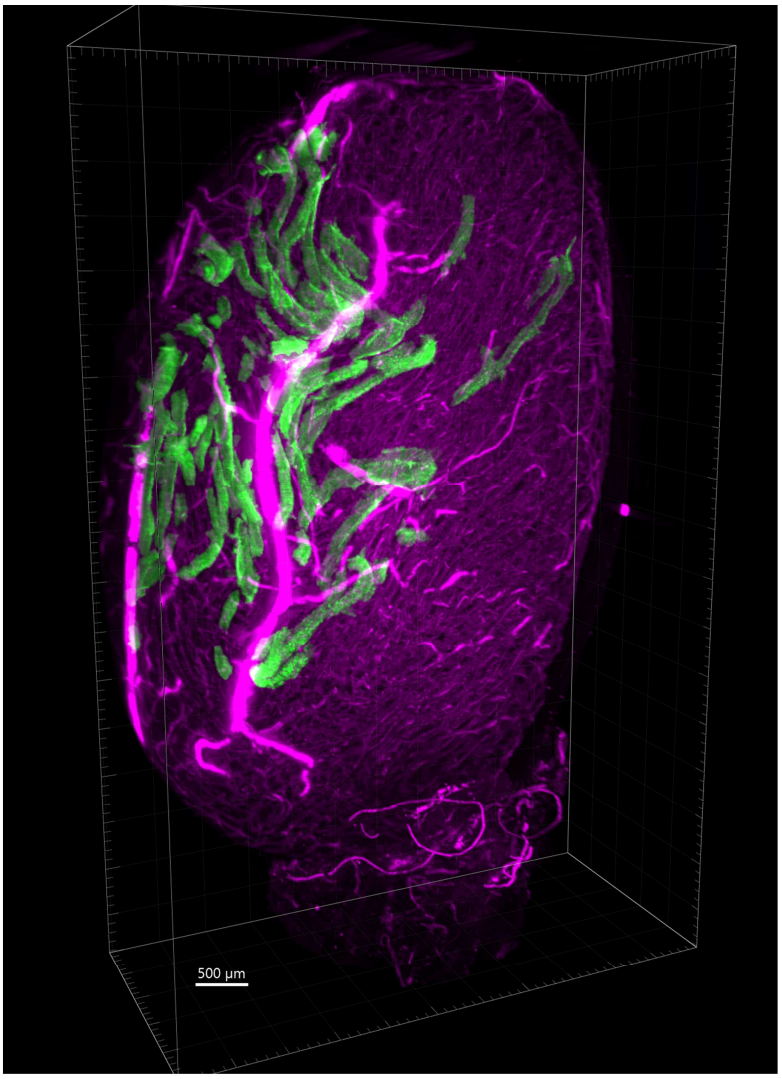

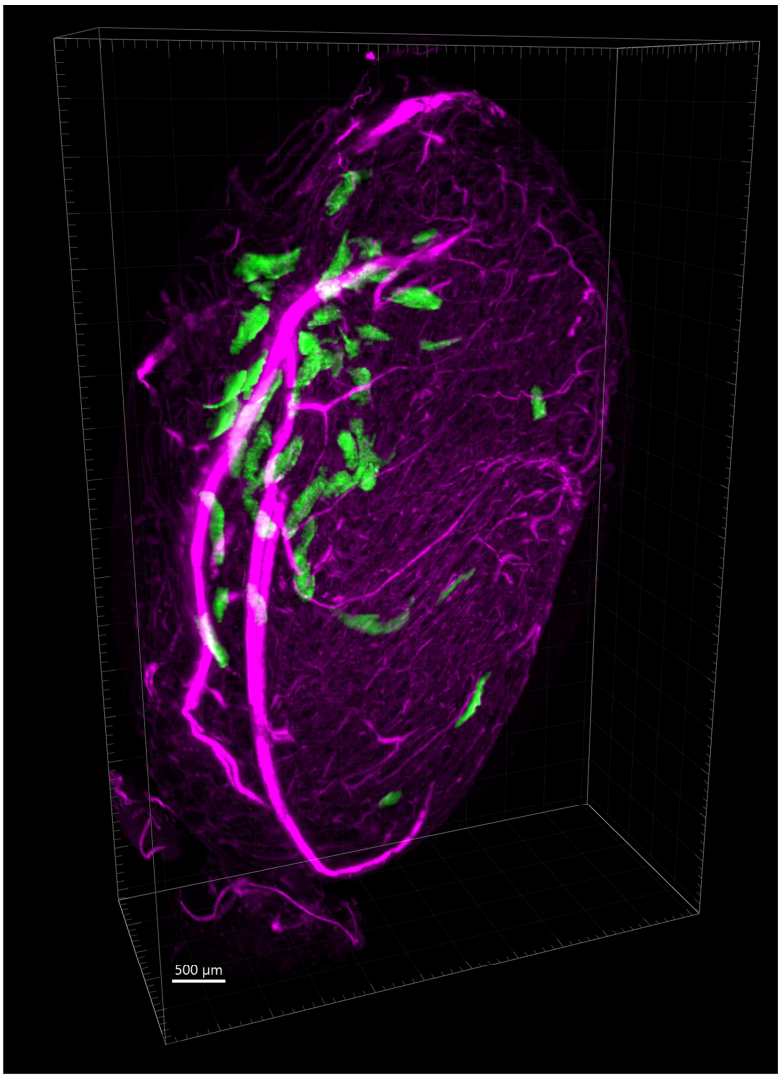

Face A **Face B**

Figure 6, Vilpreux et al 2023

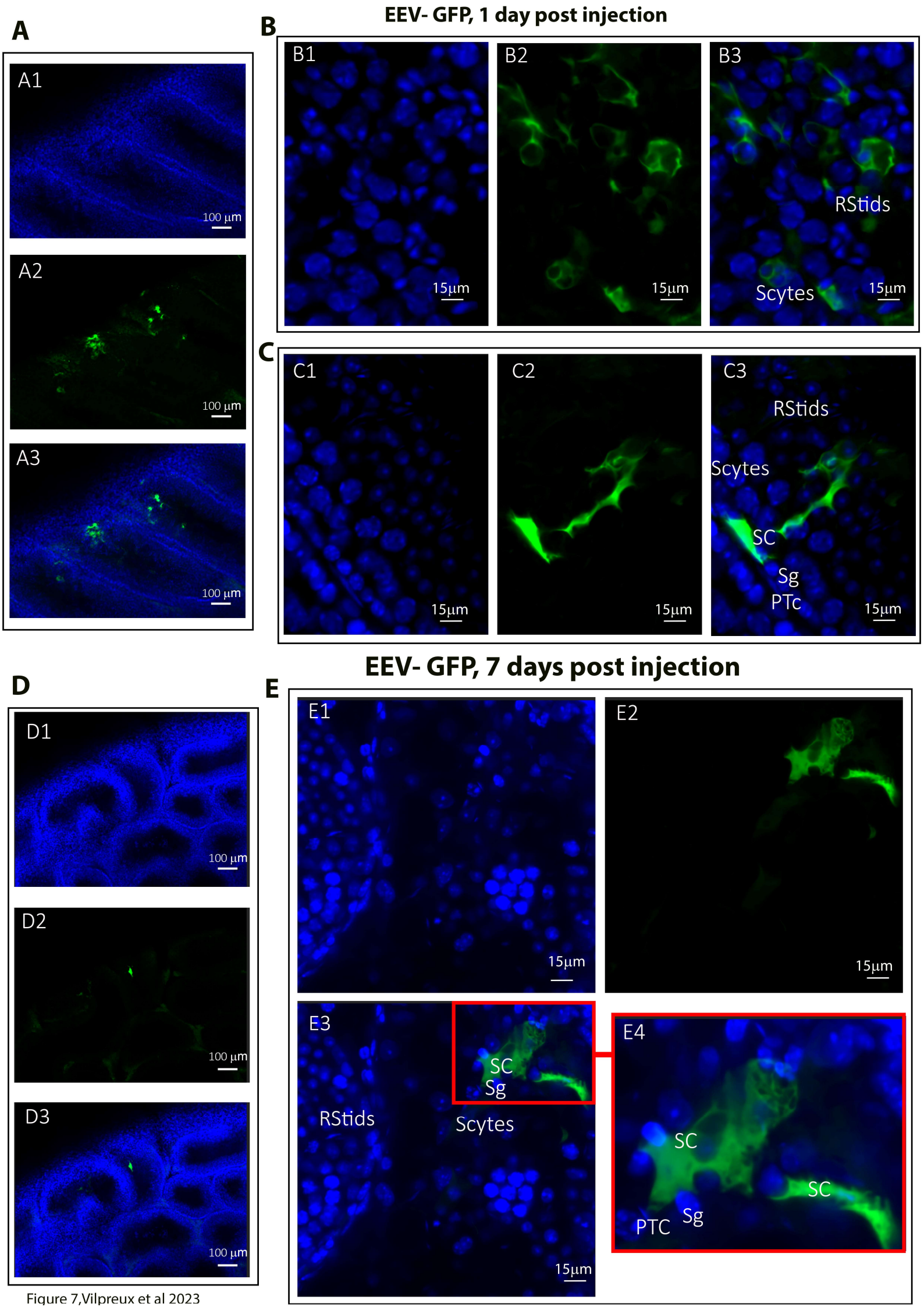

Figure 7,Vilpreux et al 2023

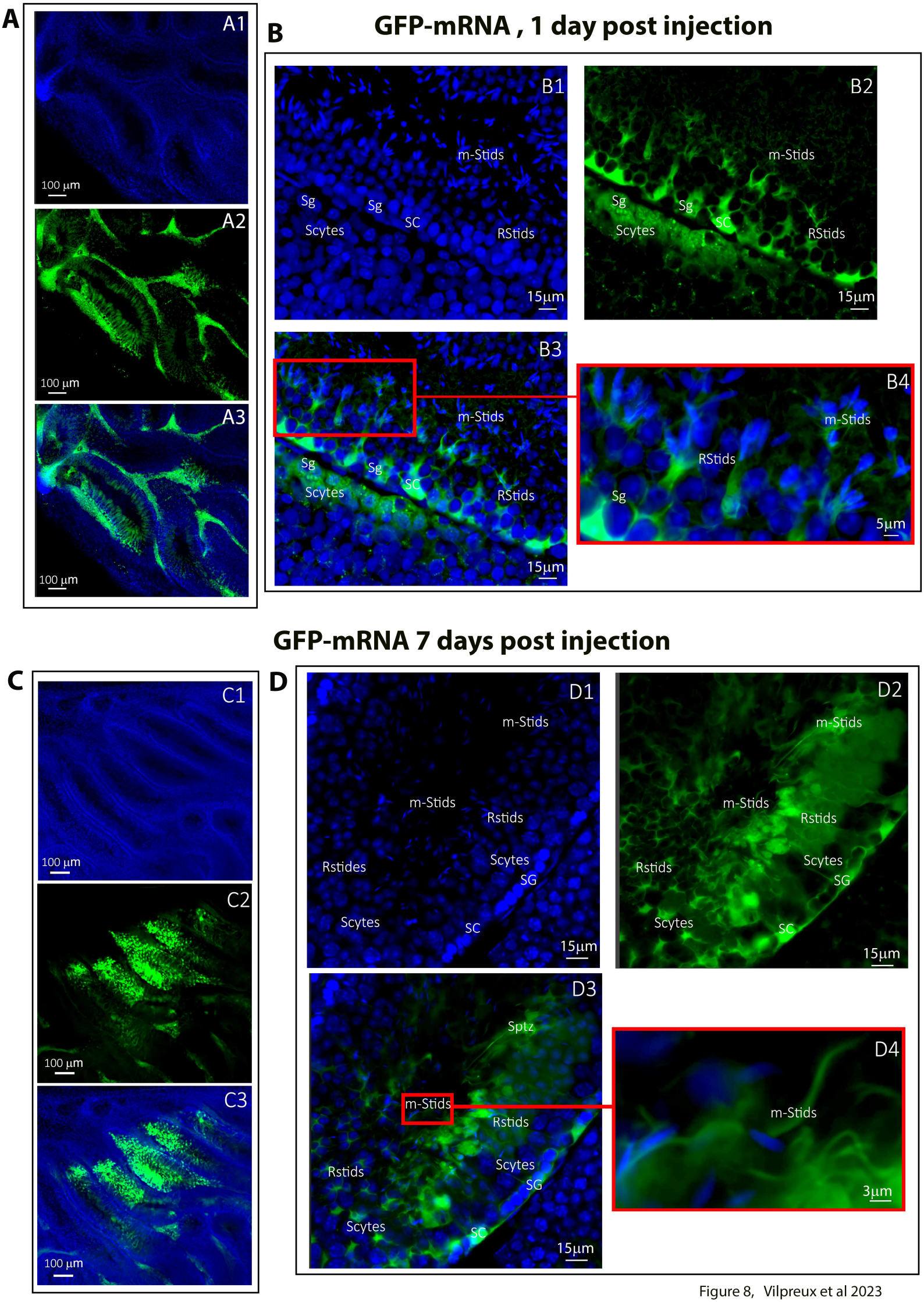

Figure 8, Vilpreux et al 2023

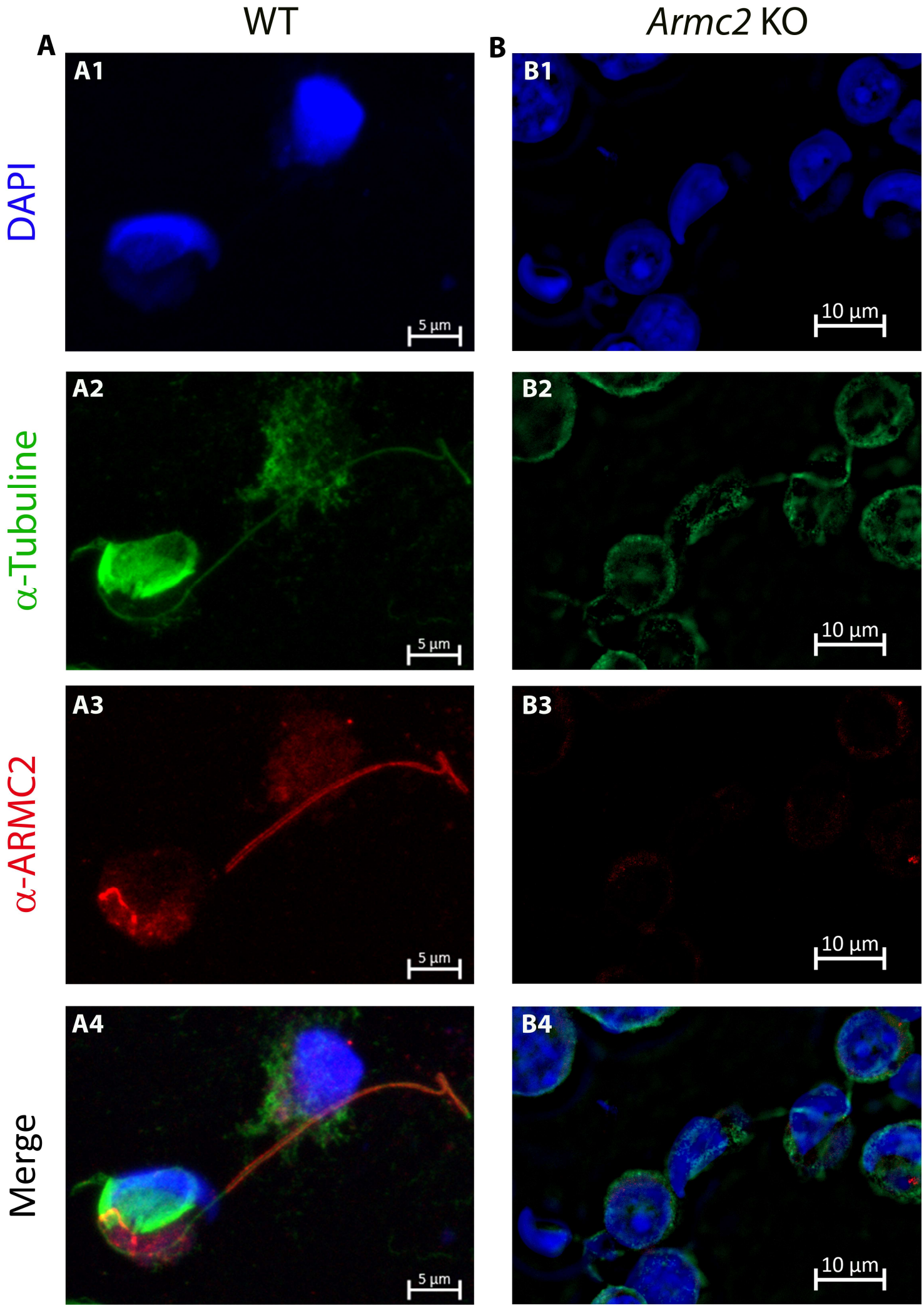

Figure 9, Vilpreux et al 2023

A

Control, 7 day post injection

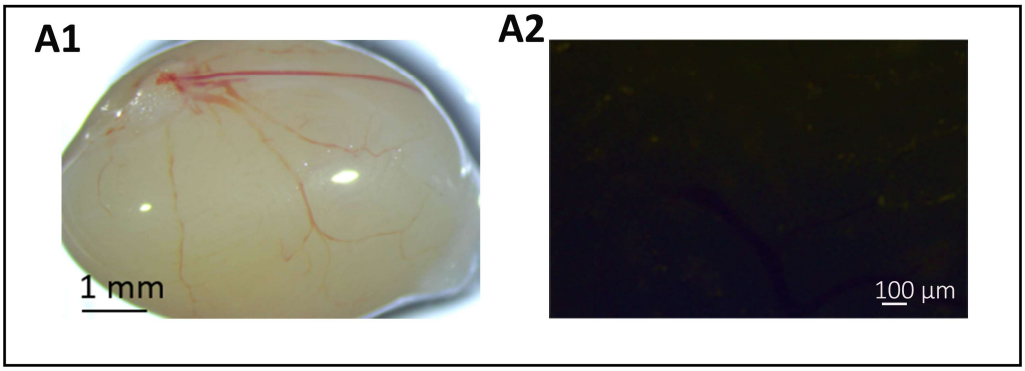

B

Armc2-mRNA + eGFP-mRNA, 7 day post injection

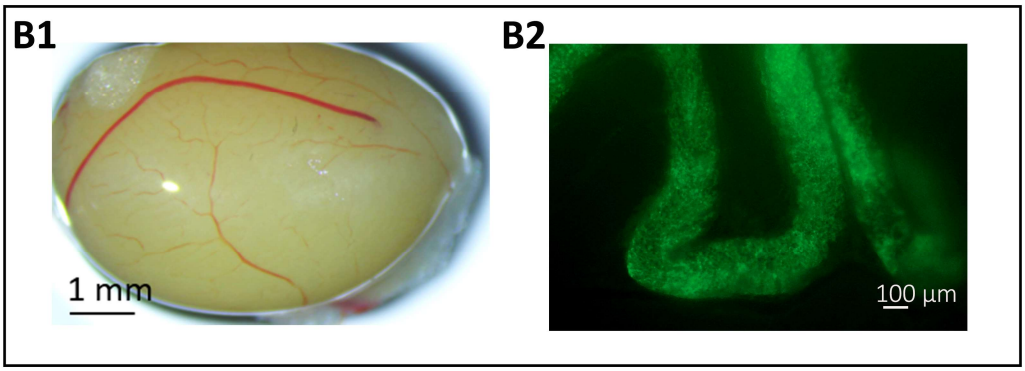

C

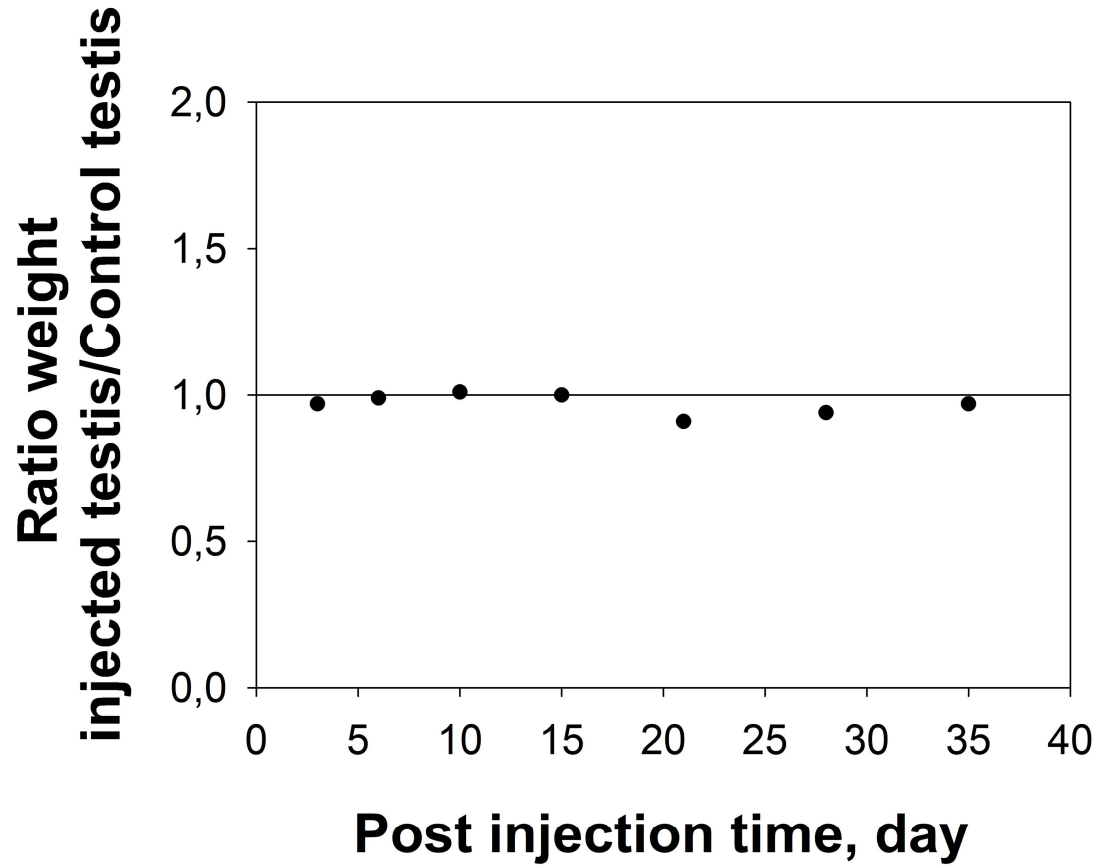

Figure 10, Vilpreux et al 2023

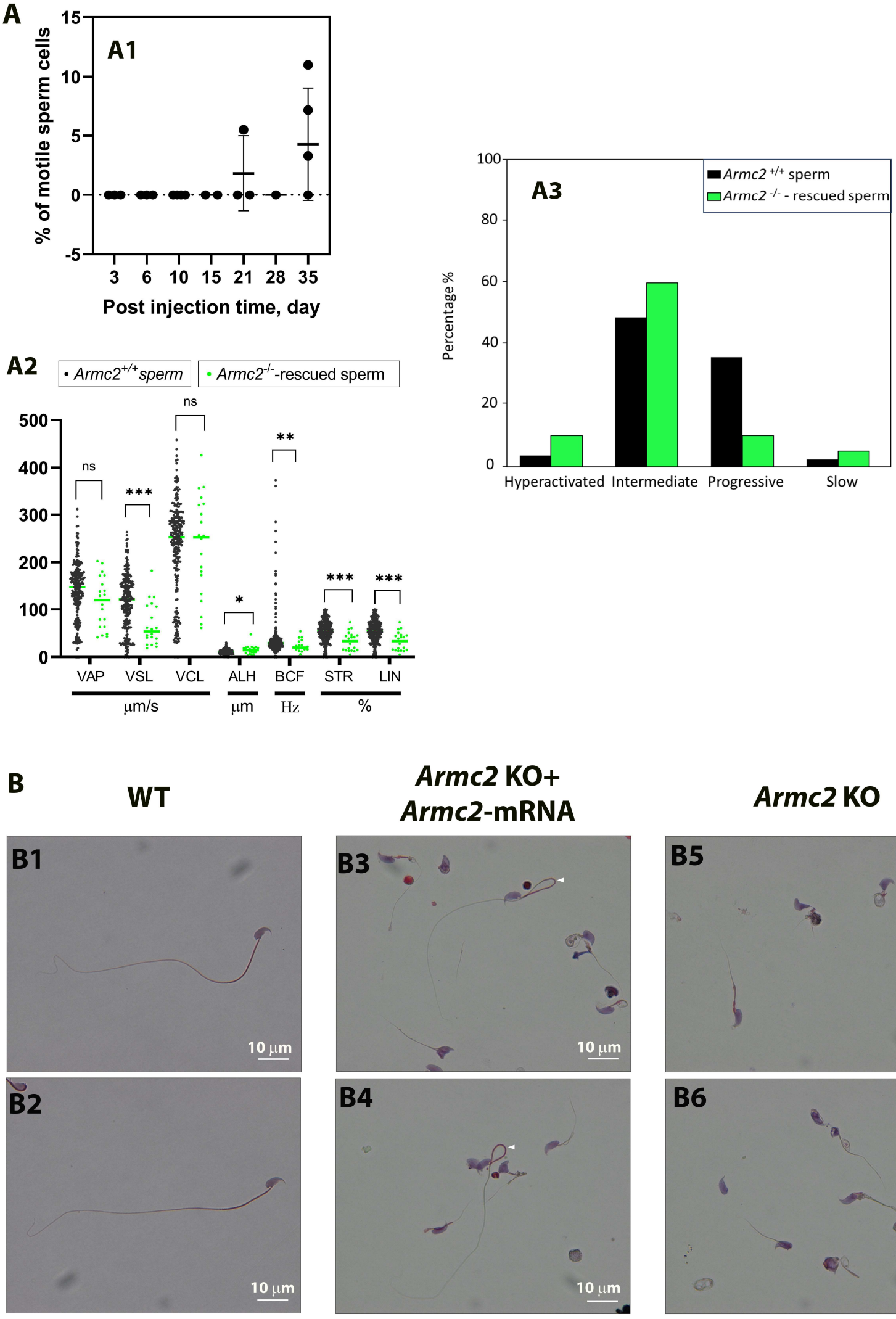

Figure 11,Vilpreux et al 2023

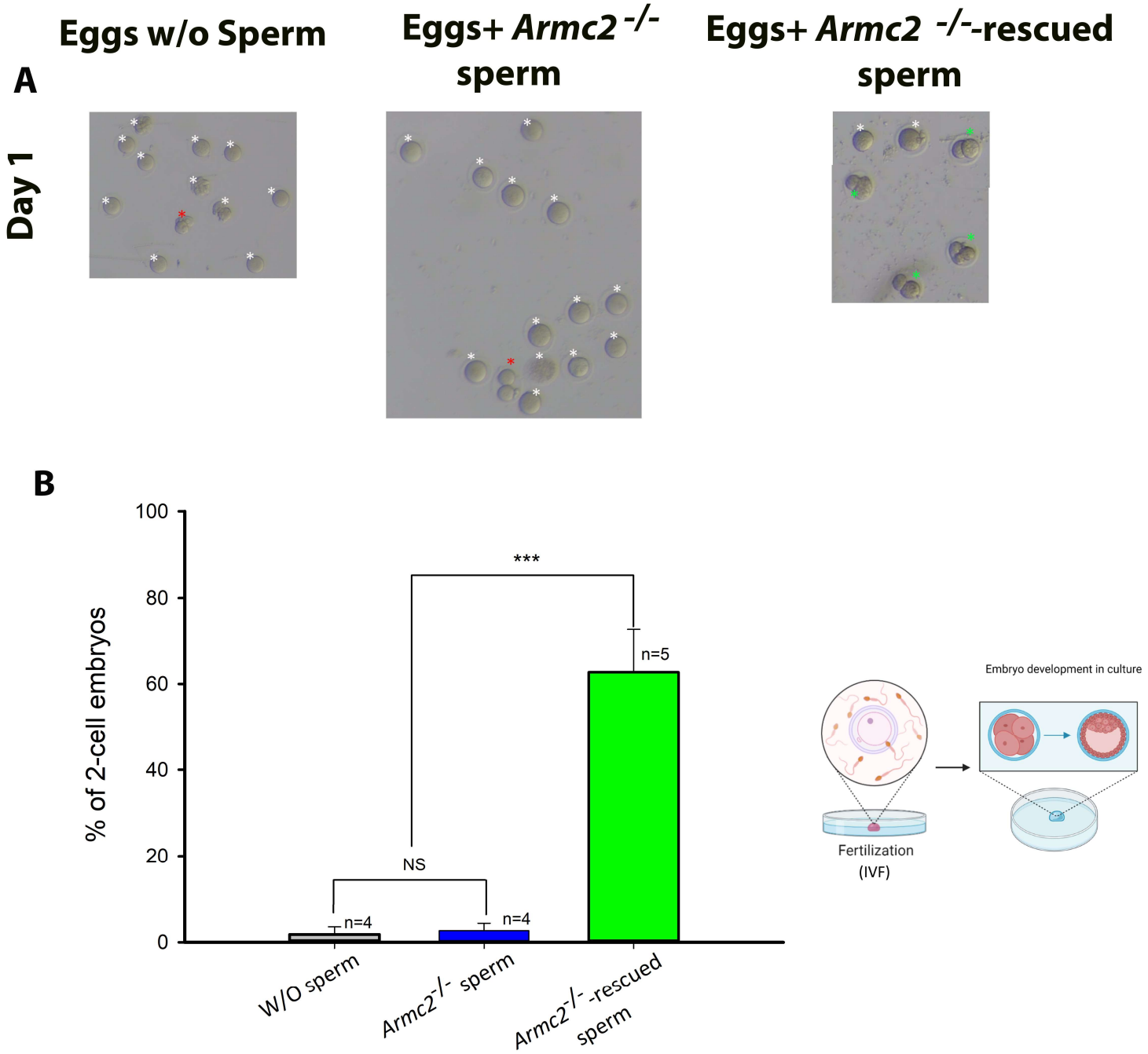

Figure 12, Vilpreux et al 2023

A

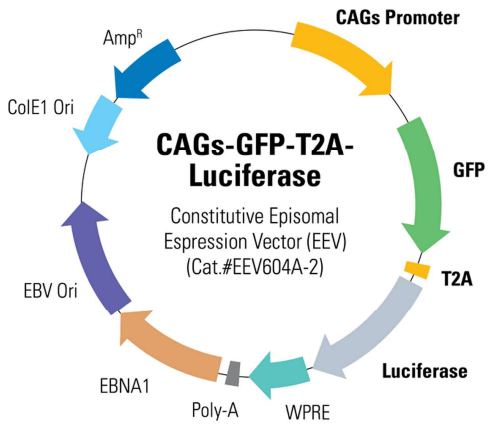

B

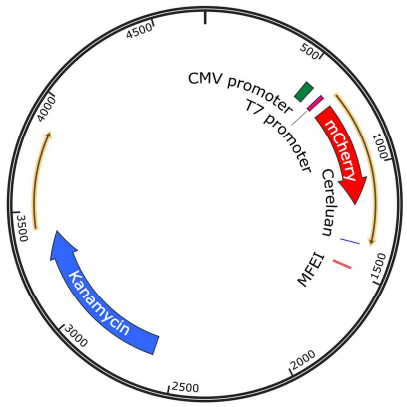

C

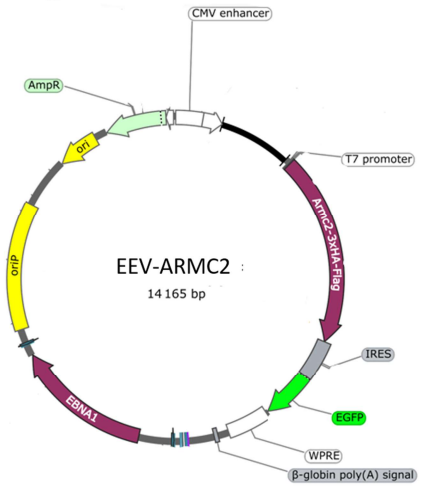

D

	1	2	3
mCherry-mRNA	+	+	+
DNAse	-	+	+
PolyA	-	-	+

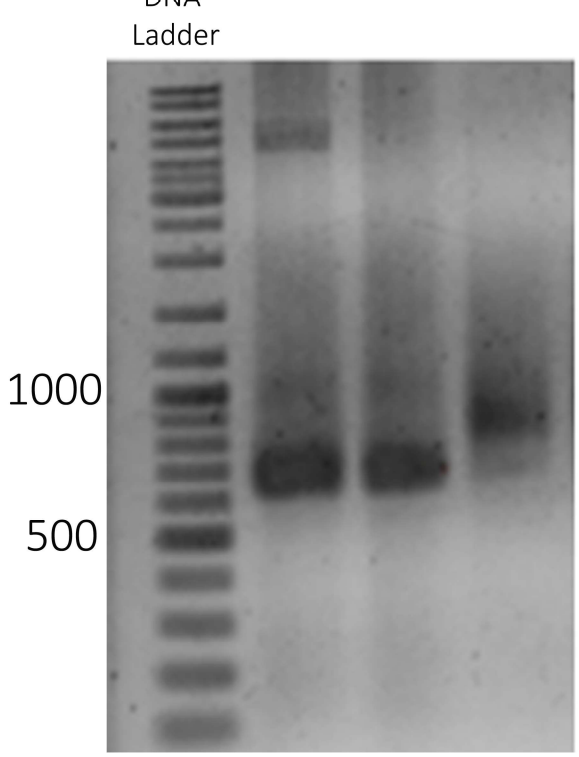

Supp Fig 1 ,Vilpreux et al 2023

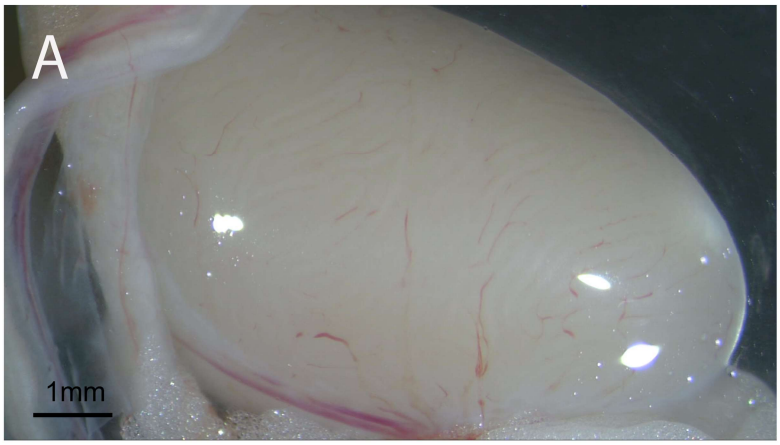

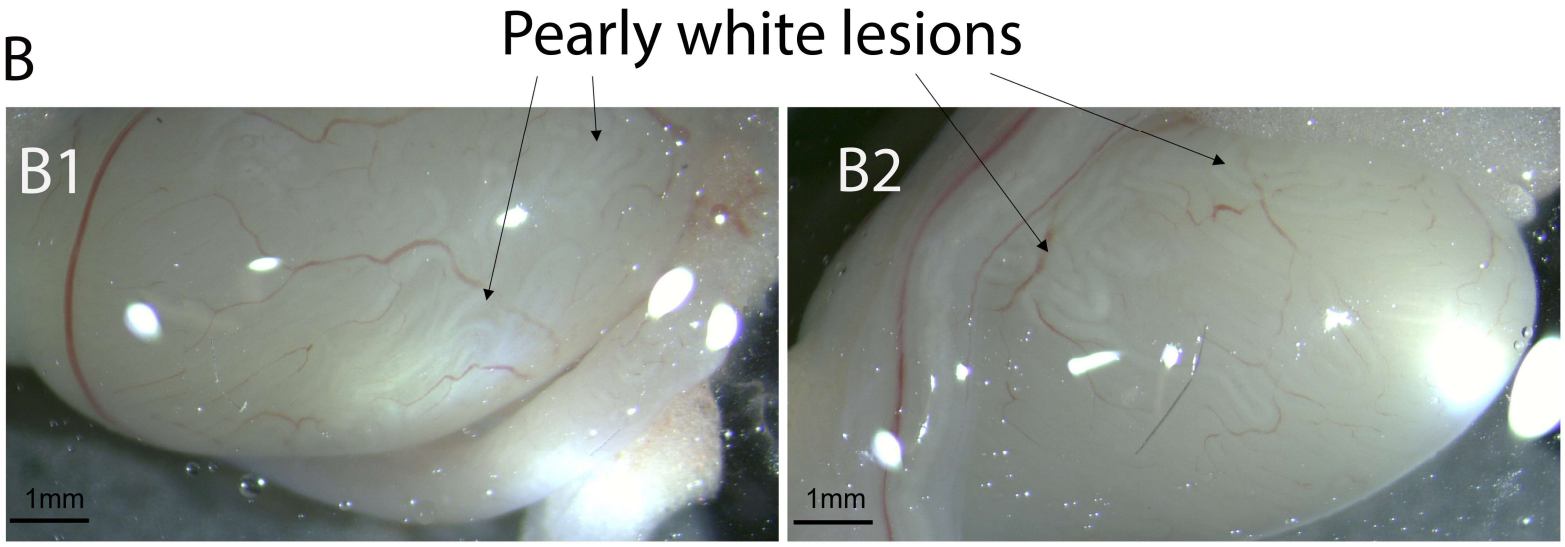

Supp Fig 2 , Vilpreux et al 2023

mCherry-mRNA

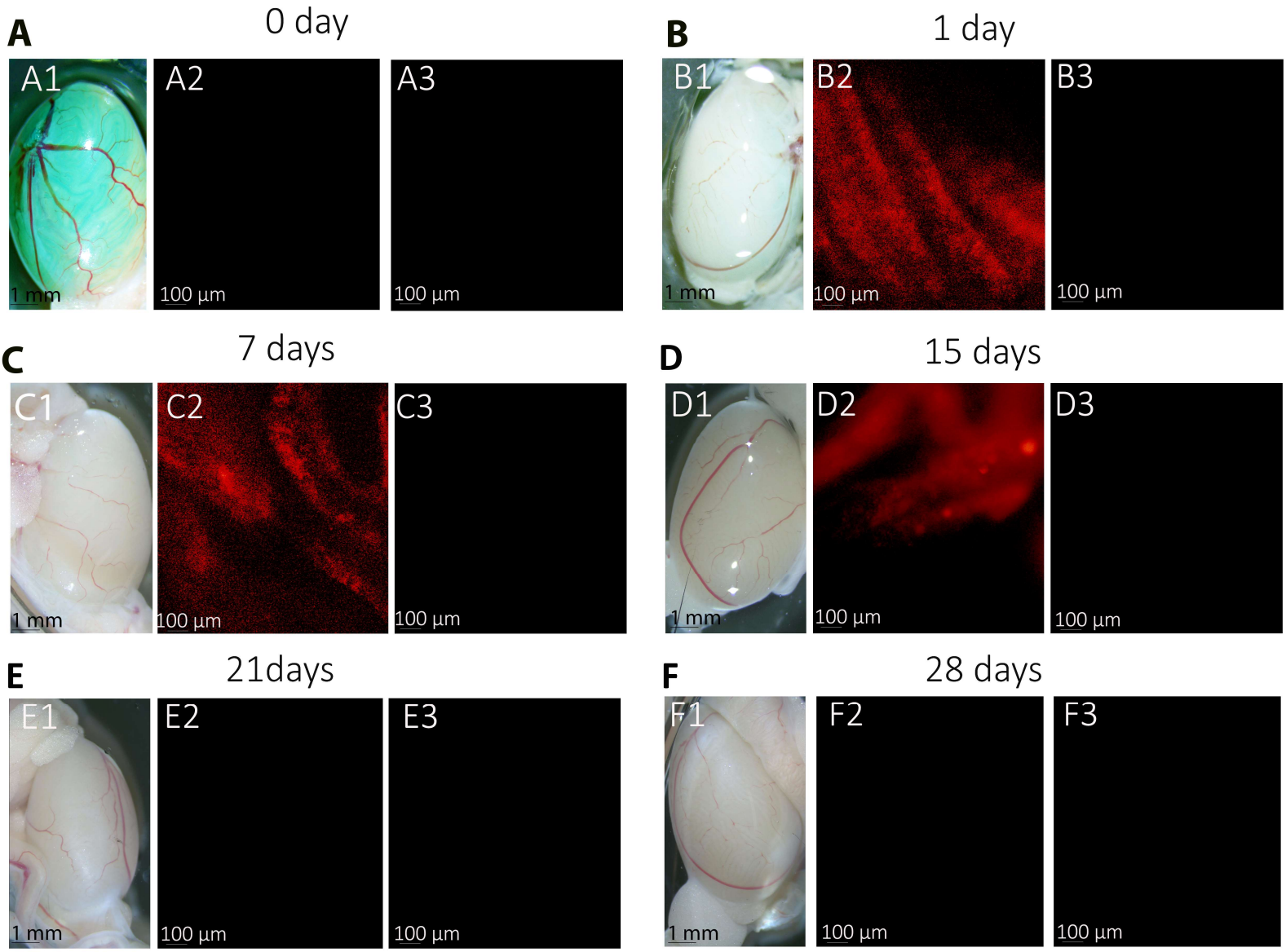

Supp Fig 3, Vilpreux et al 2023

mCherry-mRNA , 1 day post injection

A

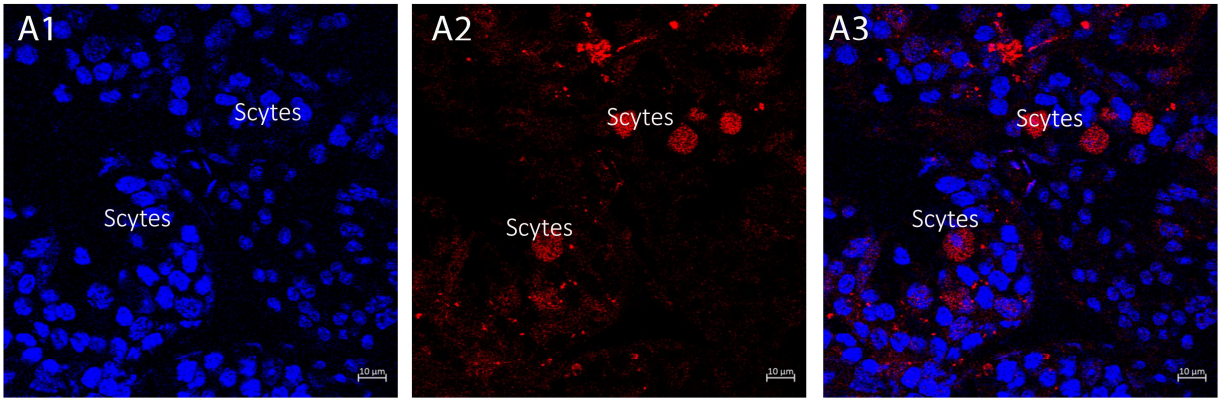

B

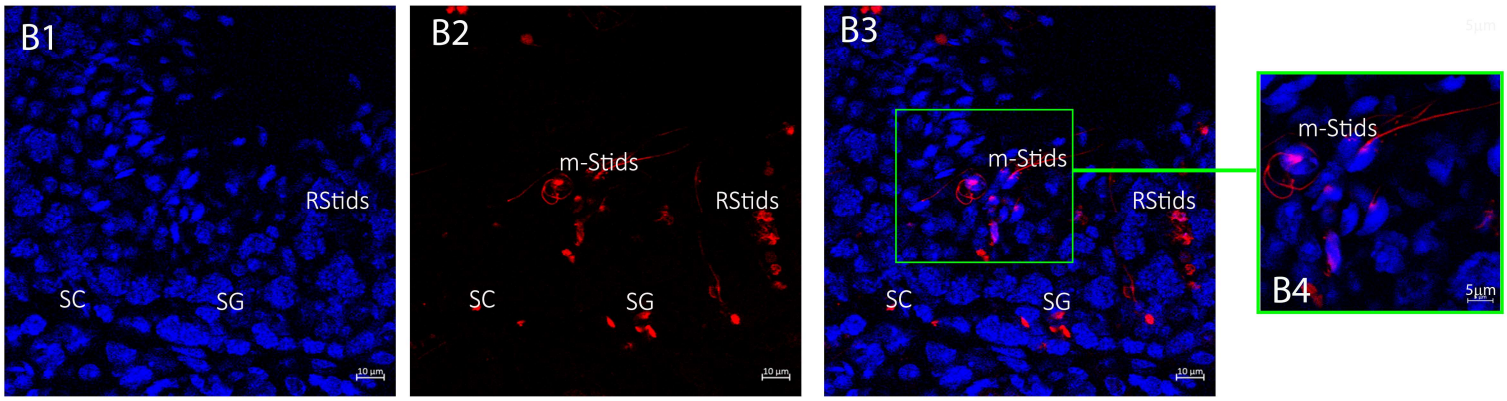

mCherry-mRNA, 7 days post injection

C

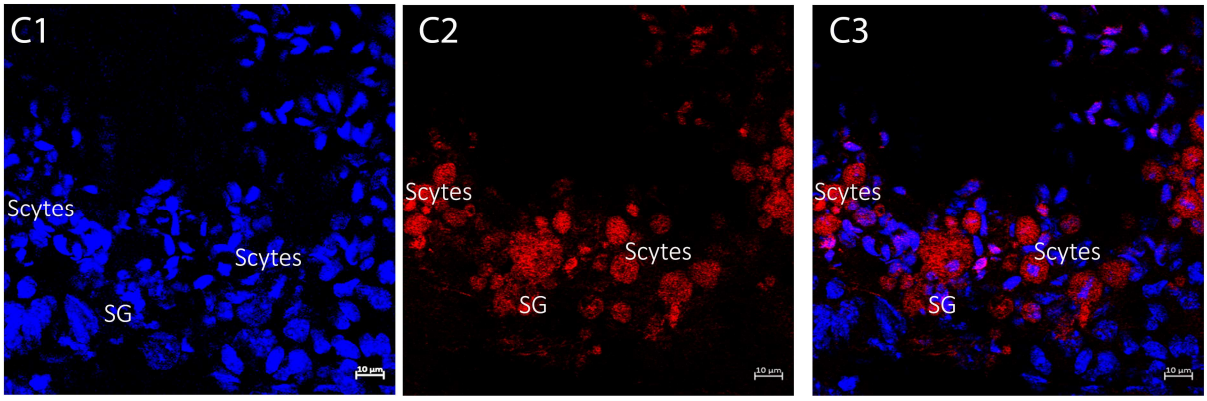

D

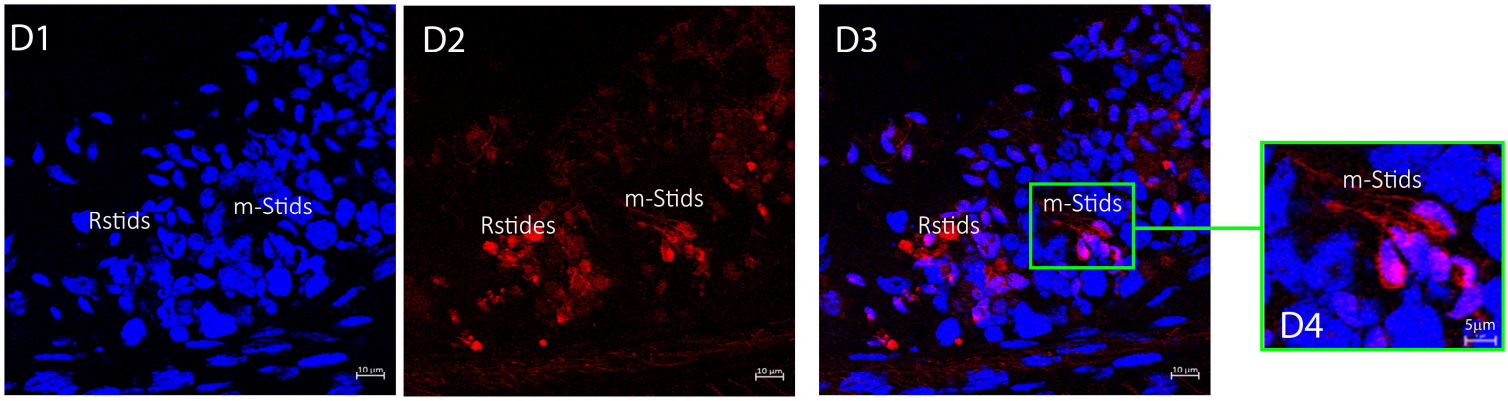

Supp Fig 4, Vilpreux et al 2023

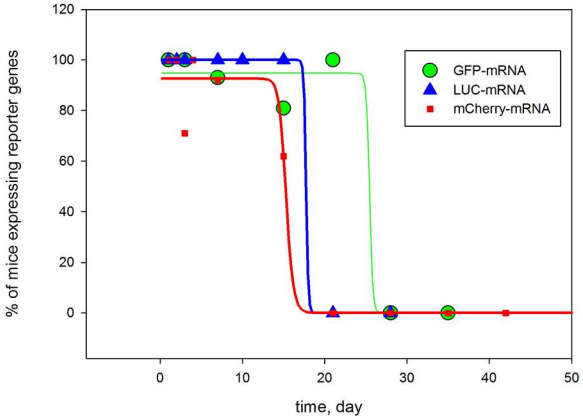

Supp Fig 5, Vilpreux et al 2023

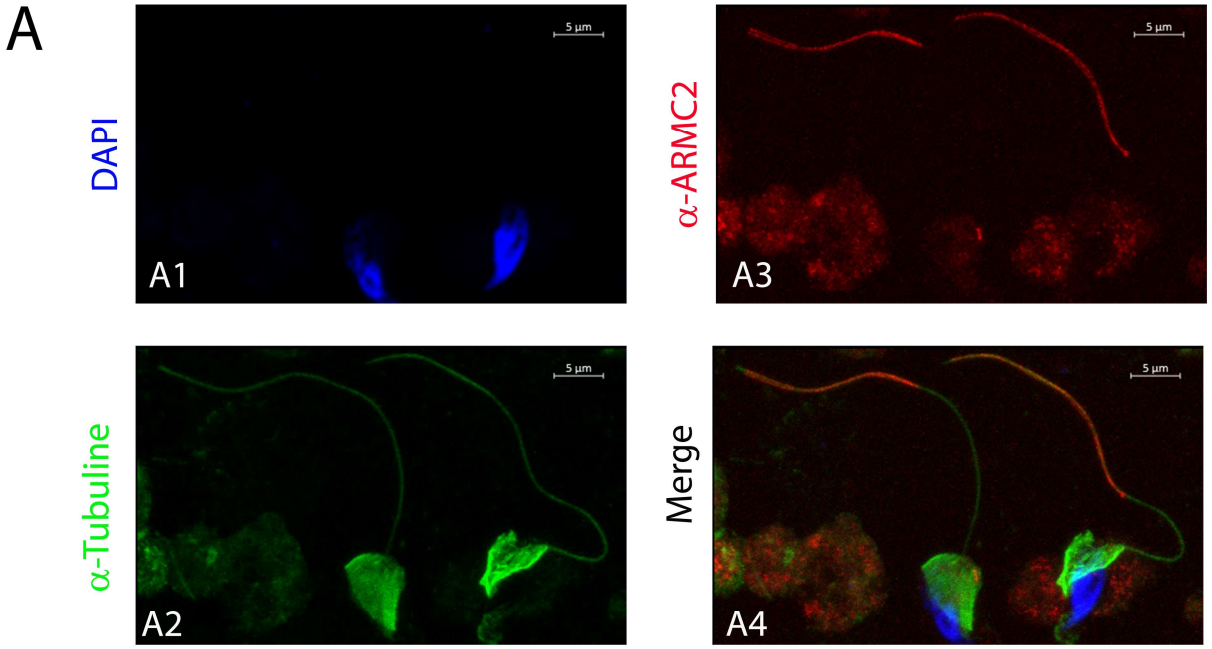

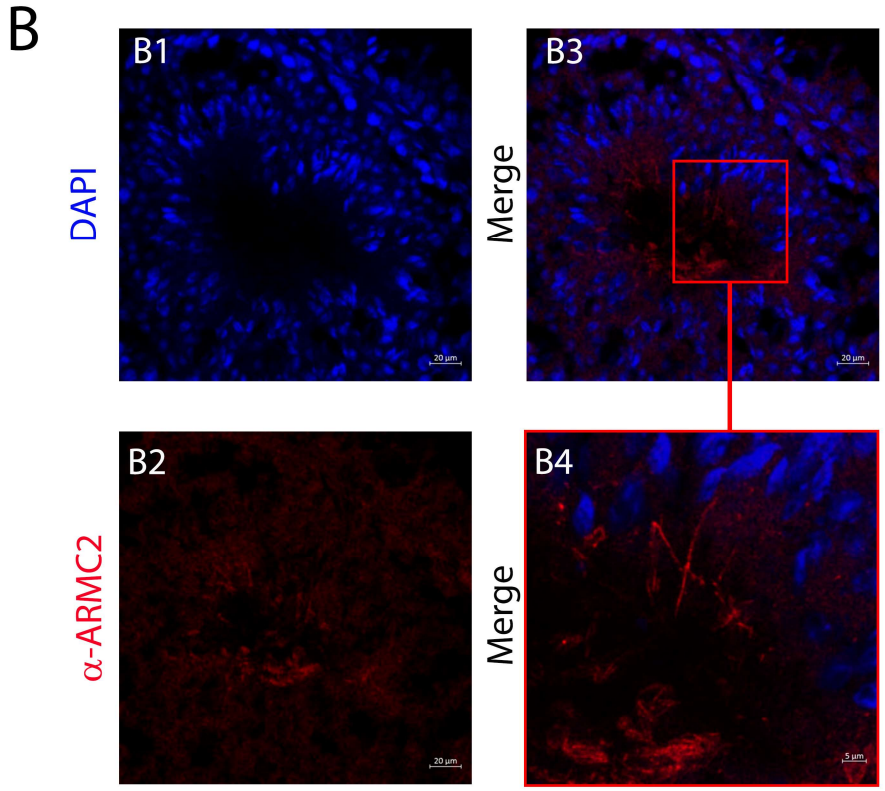

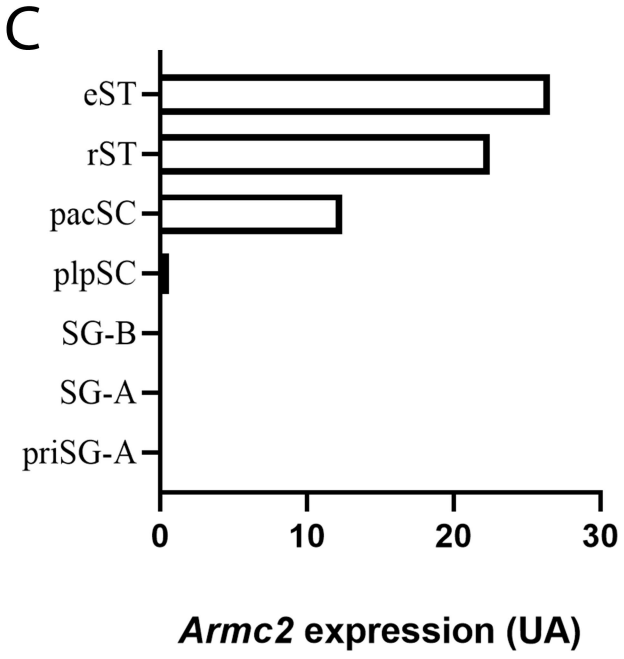

Supp Fig 6, Vilpreux et al 2023

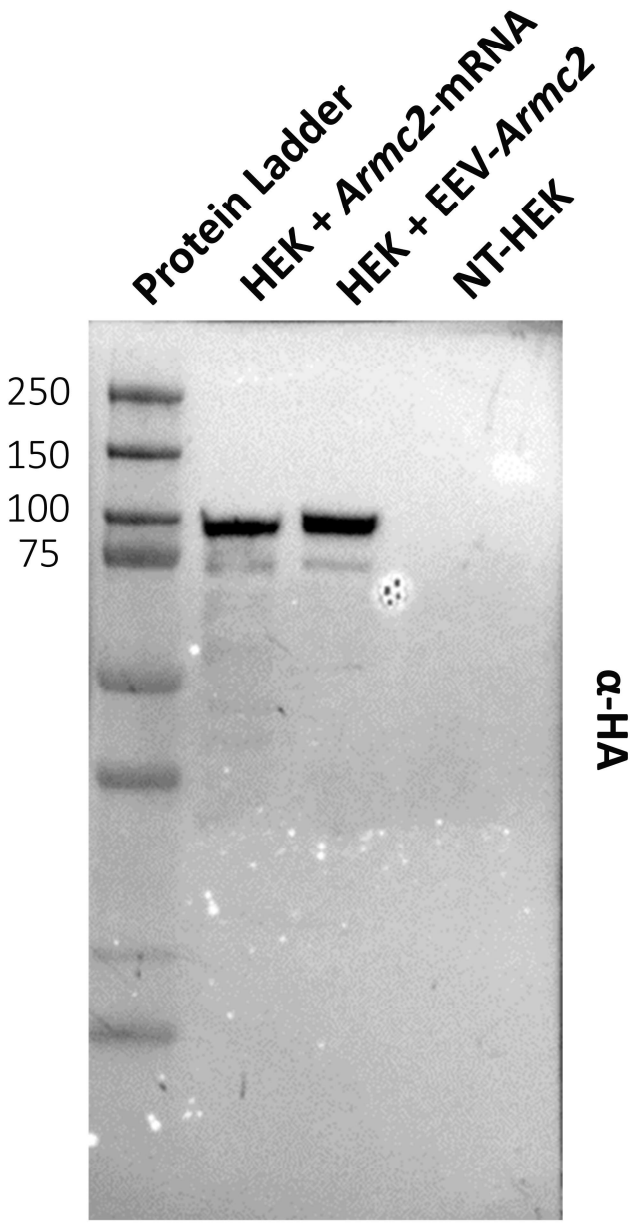

Supp Fig 7, Vilpreux et al 2023

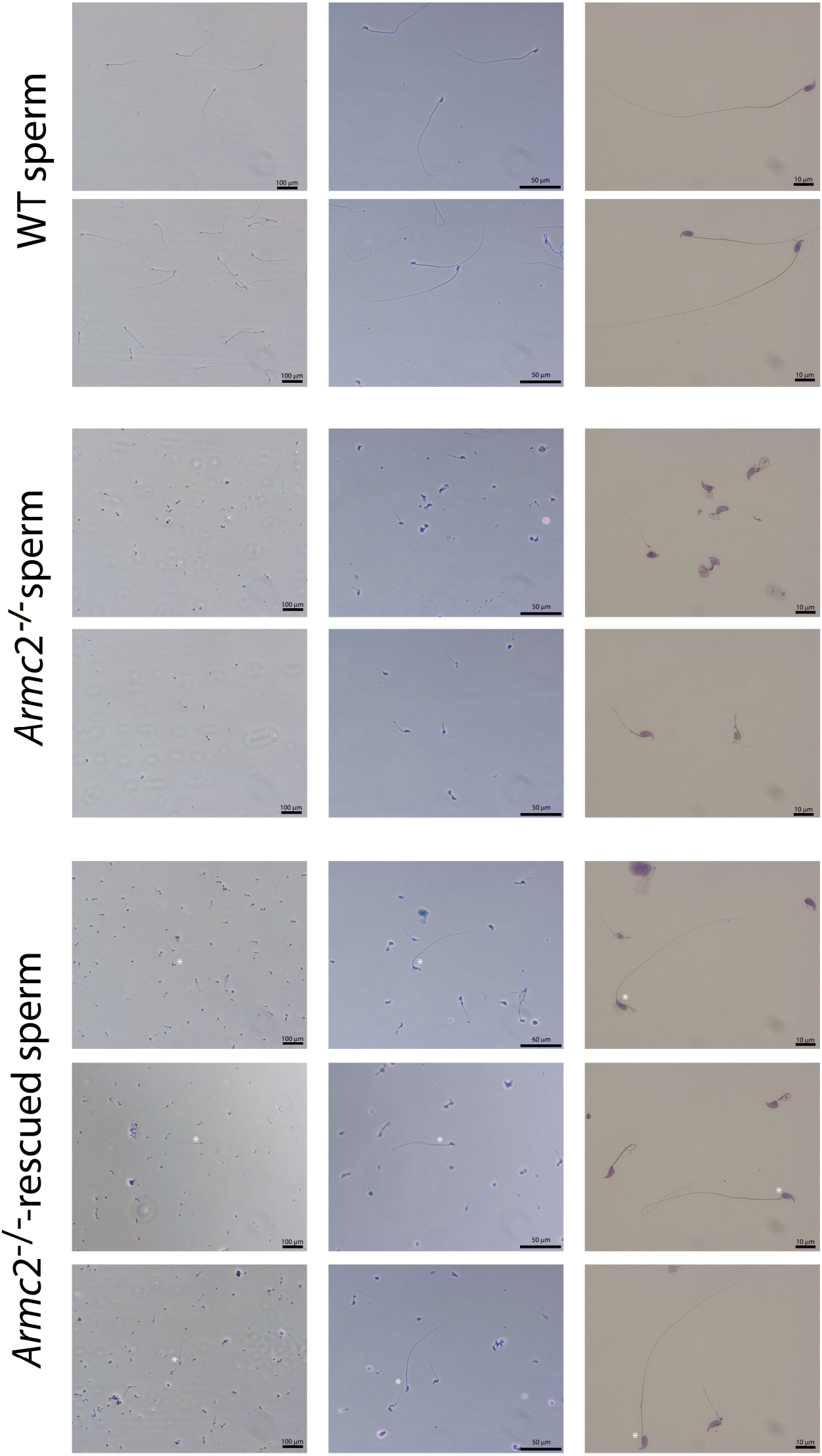

Supp Fig 8,
Vilpreux et al 2023

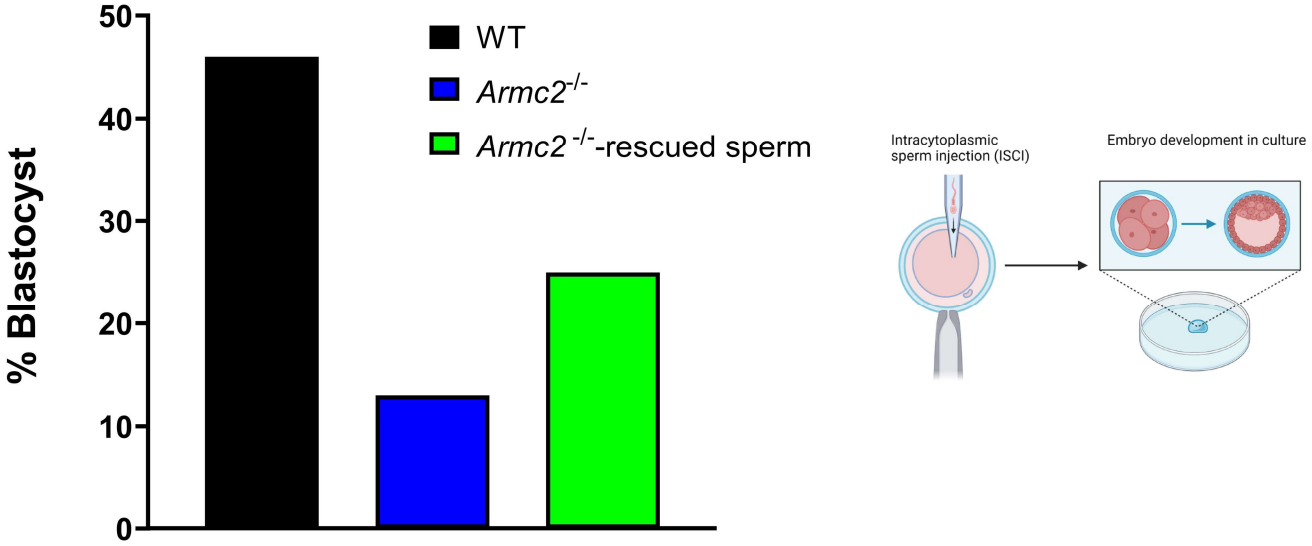

Supp Fig 9, Vilpreux et al 2023